CDF Note 10223

Combined Upper Limit on Standard Model Higgs Boson Production in up to 5.9 fb^{-1} of Data

The CDF Collaboration
URL http://www-cdf.fnal.gov
(Dated: September 28, 2010)

This note describes a combination of searches for the Standard Model Higgs boson at CDF. The ten major analyses combined are the $WH \to \ell\nu b\bar{b}$ channels, the $WH + ZH \to \not{E}_T + b\bar{b}$ channels, the $ZH \to \ell^+\ell^- b\bar{b}$ channels, the $H \to \tau^+\tau^-$ channels, the $H \to \gamma\gamma$ channel, the $WH + ZH \to jj + b\bar{b}$ channels, the $H \to W^+W^- \to \ell^+\nu_l\ell'^-\bar{\nu}_{\ell'}$ opposite-sign channels, the $WH \to WW^+W^-$ same-sign dilepton channel, the $WH \to WW^+W^-$ trilepton channels, and the the $H \to W^+W^-$ tau channels. The integrated luminosity ranges between 2.3 fb^{-1} and 5.9 fb^{-1}, depending on the channel. The 95% CL upper limit on $R = \sigma_H/\sigma_{H,SM}$ is computed as a function of m_H from 100 to 200 GeV/c^2 in steps of 5 GeV/c^2, assuming Standard Model decay branching fractions of the Higgs boson and that the ratios of the rates for the WH, ZH, $gg \to H$ and vector-boson fusion $qq \to Hqq$ production mechanisms are those predicted by the Standard Model. The results are in good agreement with those expected in the background-only hypothesis, and the observed (expected) limits on R are 1.79 (1.90) and 1.13 (1.00) at Higgs boson masses of 115 and 165 GeV/c^2, respectively.

Preliminary Results for the ICHEP 2010 Conference

I. INTRODUCTION

A combination of the results of several Higgs boson search analyses provides many advantages. Since the decay branching ratios of the Standard Model (SM) Higgs boson are strong functions of its mass m_H, the different search channels contribute in a complementary way to the sensitivity at different m_H. Some analyses seek the Higgs boson in the same decay mode but with different production mechanisms, and hence require separate treatments of the signals and backgrounds. Since these analyses all seek the same particle, the best results are obtained by combining the searches together.

A previous combination [1] has been performed using the results of the main searches for the Standard Model Higgs boson at CDF, the $WH \to \ell\nu b\bar{b}$ channels, the $WH + ZH \to \not{E}_T + bb$ channels, the $ZH \to \ell^+\ell^- b\bar{b}$ channels, the $H \to \tau^+\tau^-$ channel, the $H \to W^+W^- \to \ell^+\nu_\ell\ell'^-\bar{\nu}_{\ell'}$ channels, and the $WH + ZH \to jjb\bar{b}$ channel. This note presents an update of the combination, using the Summer 2010 versions of each analysis with more luminosity and analysis improvements, and also introducing new $VH \to VW^+W^-$ trilepton channels, $H \to W^+W^-$ channels in which one of the W bosons decays to a tau lepton, and a $H \to \gamma\gamma$ channel. The analyzed luminosities and references to the documentation are provided in Table I.

In order to combine the results of the ten search analyses, assumptions must be made about the model to be tested. The model tested by the individual analyses is a model in which Standard Model Higgs boson production proceeds, but is enhanced in all production mechanisms simultaneously by a factor of R in the cross section. The decay branching fractions and the width of the invariant mass distribution of the Higgs boson are assumed to be those predicted by the Standard Model. Exotic models which change the Higgs boson production cross section may not follow this pattern. If a fourth generation of fermions exists, for example, it would enhance the $gg \to H$ production cross section by a factor of roughly 9 [2–4], but would not enhance the WH and ZH associated production mechanisms. A heavy neutrino in the fourth generation may take some of the Higgs boson decay branching ratio if it is light enough to be a decay product of the Higgs boson.

II. SIGNAL PRODUCTION AND DECAY MODEL

We normalize our Higgs boson signal predictions to the most recent high-order calculations available. The $gg \to H$ production cross section is calculated at NNLO in QCD with NNLL soft-gluon resummation, and also includes two-loop electroweak effects and handling of the running b quark mass [5, 6]. These calculations are refinements of the earlier NNLO calculations of the $gg \to H$ production cross section [7–9]. Electroweak corrections were computed in Refs. [10, 11]. Soft gluon resummation was introduced in the prediction of the $gg \to H$ production cross section in Ref. [12].

The $gg \to H$ production cross section depends strongly on the gluon parton density function, and the accompanying value of $\alpha_s(q^2)$. The cross sections used here are calculated with the MSTW 2008 NNLO PDF set [13]. The Higgs boson production cross sections are listed in Table II. We include the larger theoretical uncertainties due to scale variations and PDF variations separately for each jet bin for the $gg \to H$ processes as evaluated in Ref. [14]. The analyses which seek the $gg \to H$ production mechanism, namely the $H \to \tau^+\tau^-$ and $H \to W^+W^-$ analyses, separate events into categories based on the number of jets accompanying the Higgs boson candidate's decay products. We treat the scale uncertainties as 100% correlated between the predictions of the Higgs boson cross section in the different jet bins, and also treat the PDF uncertainties as 100% correlated between jet bins.

We include all significant Higgs production modes in the high-mass search. Besides the gluon-gluon fusion mechanism described above, we include Higgs boson production in association with a W or Z vector boson (VH), and vector-boson fusion (VBF). Our WH and ZH cross sections are from Ref. [15]. Earlier calculations of the WH and ZH cross section are available in [16–18]. The VBF cross sections are available in [16, 19]. For the low-mass searches, we target the WH, ZH and VBF production modes with specific searches, including also those signal components not specifically targeted but which fall in the acceptance nonetheless. Our low-mass $H \to \tau^+\tau^-$ and $H \to \gamma\gamma$ searches also include the $gg \to H$ process in their signal predictions.

In order to predict the distributions of the kinematics of Higgs boson signal events, we use the PYTHIA [20] Monte Carlo program, with CTEQ5L [21] leading-order (LO) parton distribution functions. The Higgs boson decay branching ratio predictions are calculated with HDECAY [22], and are also listed in Table II. We use HDECAY Version 3.53.

III. SEARCH CHANNELS

Updates and improvements have been made to the channels and the combination since the previous combination [1], and are listed below.

- As before [1], the $WH \rightarrow \ell\nu b\bar{b}$ channel is split into the two-jet and three-jet categories. The W+two-jet channels are analyzed with a neural network [23] and are split into twelve categories, based on the b-tagging method and the lepton requirements. The b-tagging categories for the two jets are double-tight SECVTX (TDT), Tight SECVTX+JetProb (LDT), Tight SEVTX+Roma (LDTX), and Tight SECVTX+no other tag (ST). The SECVTX b-tagging algorithm is described in Reference [24], and the JetProb b-tagging algorithm is described in Reference [25]. The lepton categories are tight central letpons, plug electrons, and isolated tracks. There are six three-jet channels using a matrix-element-based search discriminant [26] and twelve two-jet channels. The three-jet channels are itemized by the b-tag category – double-tight SECVTX (TDT), tight SECVTX+JetProb (LDT), and a single-tight SECVTX tag where the other jet is not tagged by any algorithm (ST). There are two lepton categories for the three-jet WH channels, central trigger leptons and extended muon coverage, which relies on the missing-E_t+jets trigger. The two-jet channels have been updated for a total of 5.7 fb^{-1} of analyzed luminosity, and the three-jet channels have been updated for a total of 5.6 fb^{-1} of integrated luminosity.

- The $ZH \rightarrow \ell^+\ell^- b\bar{b}$ search now includes six new channels using looser muon selection criteria (CMIO) [27]. The six channels are broken down by b-tag category: single SECVTX (ST), double SECVTX (TDT), and Loose SECVTX+JetProb (LDT), and whether the events are collected on the high-P_T muon trigger path or the $\not\!\!E_T$ trigger path. The binning of the two-dimensional discriminant outputs for the main $ZH \rightarrow \ell^+\ell^- b\bar{b}$ [28] and the looser muon versions [27] has been optimized for more robust predictions of the expected signal and background in the highest signal-to-background bins as well as to collect together sparsely populated low signal-to-background bins.

- A search for $H \rightarrow \gamma\gamma$ [29] is now included, analyzing 5.4 fb^{-1} of data.

- The $H \rightarrow W^+W^-$ channels now include dedicated searches for the cases in which one of the W bosons decays to a hadronically decaying tau lepton. Three new trilepton channels have been added since the previous combination [1] in order to separate $WH \rightarrow WWW$ and $ZH \rightarrow ZWW$ events in which three charged leptons are in the final state. Events with three identified leptons are grouped into channels depending on whether a pair of leptons has an invariant mass close to M_Z, and also based on how many jets there are in the event. All $H \rightarrow W^+W^-$ channels have been updated to include 5.9 fb^{-1}.

- An update of the $p\bar{p} \rightarrow H + 2$ jets $\rightarrow \tau^+\tau^- + 2$ jets channel is included in this combination, analyzing 2.3 fb^{-1} of data.

- The $WH + ZH \rightarrow b\bar{b}jj$ channel is updated with 4.0 fb of data, now splitting the candidates into four channels. Two of these four channels are new, accepting events for which the non-b-tagged jets have an invariant mass higher than 120 GeV/c^2 in order to capture the VBF signal, while the other two channels target events with associated production of a Higgs boson with a W or Z boson and require this invariant mass to be between 50 and 120 GeV/c^2. Both of these categories of events are further subdivided by b-tagging category – two tight SECVTX tags or one tight SECVTX tag and one JetProb tag.

- the $WH, ZH \rightarrow \not\!\!E_T b\bar{b}$ analysis [30] is updated with 5.7 fb^{-1} of data. The W, Z+jets background prediction is now made with ALPGEN [32] instead of PYTHIA [20]. The same tag categories, TDT, LDT, and ST are defined as in the previous version of the analysis [31].

The mass grid for the $H \rightarrow W^+W^-$ channels is in 5 GeV/c^2 steps between $m_H = 110$ GeV/c^2 and 200 GeV/c^2. For the lower mass points, the $H \rightarrow b\bar{b}$ and $H \rightarrow \tau^+\tau^-$ searches dominate the sensitivity. The mass grid for these searches is in 5 GeV/c^2 steps between $m_H = 100$ GeV/c^2 and 150 GeV/c^2.

IV. COMBINATION METHOD

A Bayesian technique is used to compute the observed and expected upper limits on R. The prior is flat in the product of R and the total expected signal yield after all efficiencies and acceptances are taken into account. This prior was used in the previous combination [1].

A. Common Parameter Alignment

The individual channel analyses listed above require theoretical input in the form of kinematic distributions from Monte Carlo (usually from leading-order generators with parton shower models), and higher-order predictions of inclusive cross sections. The method of inclusion of systematic uncertainties, described below, takes advantage of shared dependence on common parameters, such as the luminosity, the $t\bar{t}$ and single-top cross sections, the diboson cross sections and the vector-boson-plus-heavy-flavor-jets K factor relative to the Monte Carlo prediction.

In discussions with D0, we have made agreements to use the highest-order available calculations of the $t\bar{t}$, single top, and diboson production cross sections, computed with the MSTW2008 PDF set [13]. We have scaled each input analysis's background templates separately for each of these processes in order to align to the common parameter values.

For the $\sigma_{t\bar{t}}$ cross section, we compute its value at $m_t = 173 \pm 1.2$ GeV/c^2 [33], and use newer, higher-order calculations [34], using the MSTW2008 PDF set [13]. The channels' background templates are evaluated with $m_t = 175$ GeV/c^2, but since the kinematics are not expected to be strongly dependent on m_t, particularly in the advanced discriminants designed to separate Higgs boson events from backgrounds, only the cross section has been adjusted. We use a value of

$$\sigma_{t\bar{t}} = 7.04^{+0.24}_{-0.36}\ \text{(scale)} \pm 0.14\ \text{(PDF)} \pm 0.30\ \text{(mass) pb.} \tag{1}$$

The single top cross sections [35] are, for the s-channel,

$$\sigma_{s-\text{chan}} = 1.046 \pm 0.006\ \text{(scale)} \pm 0.059\ \text{(PDF)} \pm 0.030\ \text{(mass) pb,} \tag{2}$$

and for the t-channel,

$$\sigma_{t-\text{chan}} = 2.10 \pm 0.027\ \text{(scale)} \pm 0.18\ \text{(PDF)} \pm 0.045\ \text{(mass) pb.} \tag{3}$$

The templates from each channel have been scaled by the appropriate ratios of cross sections to unify the predictions. The above theoretical uncertainties are applied in place of those supplied by the analyses. The scale and PDF uncertainties are taken to be uncorrelated between the three processes.

The W, Z+heavy-flavor K-factors are correlated between the $WH \to \ell\nu b\bar{b}$ and the $ZH \to \ell^+\ell^- b\bar{b}$ channels, but these are considered uncorrelated with the $WH + ZH \to \not{E}_T + bb$ channels. This latter decorrelation is conservative since introducing a correlation allows one channel to constrain another channel's background.

MCFM [36] has been used to compute the NLO cross sections for WW, WZ, and ZZ production [37].

Using a scale choice $\mu_0 = M_V^2 + p_T^2(V)$ and the MSTW2008 PDF set [13], the cross section for inclusive W^+W^- production is

$$\sigma_{W^+W^-} = 11.34^{+0.56}_{-0.49}\ \text{(scale)}\ ^{+0.35}_{-0.28}\ \text{(PDF) pb} \tag{4}$$

Lowering the factorization and renormalization scales by a factor of two increases the cross section, and raising the scales by a factor of two decreases the cross section. The PDF uncertainty has the same fractional impact on the predicted cross section independent of the scale choice.

Using a scale choice $\mu_0 = M_V^2 + p_T^2(V)$ and the MSTW2008 PDF set [13], the cross section for inclusive $W^\pm Z^0$ production is

$$\sigma_{W^\pm Z^0} = 3.22^{+0.20}_{-0.17}\ \text{(scale)}\ ^{+0.11}_{-0.08}\ \text{(PDF) pb} \tag{5}$$

For the Z^0, leptonic decays are used in the definition, with both γ and Z^0 exchange. The cross section is defined in the region $75 \leq m_{\ell^+\ell^-} \leq 105$ GeV for the leptons from the neutral current exchange. Lowering the factorization and renormalization scales by a factor of two increases the cross section, and raising the scales by a factor of two decreases the cross section.

$$\sigma_{Z^0Z^0} = 1.20^{+0.05}_{-0.04}\ \text{(scale)}\ ^{+0.04}_{-0.03}\ \text{(PDF) pb} \tag{6}$$

For the diboson cross section calculations, $|\eta_\ell| < 5$ for all calculations. Loosening this requirement to include all leptons makes a $\sim$+0.4% change in the predictions. Lowering the factorization and renormalization scales by a factor of two increases the cross section, and raising the scales by a factor of two decreases the cross section.

All PDF uncertainties are computed as the quadrature sum of the 20 68% CL eigenvectors provided with MSTW2008 (MSTW2008nlo68cl).

The uncertainties on the diboson production cross sections are assumed to be 100% correlated between WW, WZ, and ZZ production.

The signal cross section uncertainties have been unified across channels. We assign separate scale and PDF uncertainties for $gg \to H$ production, in a jet-bin-dependent way, correlating the uncertainties across jet bins [14]. We assume a 5% uncertainty on WH and ZH production (correlated between WH and ZH), and a 10% uncertainty on vector-boson fusion, both independent of m_H. The theoretical uncertainties on the separate Higgs boson production mechanisms are considered to be independent of each other and of all other uncertainties.

The luminosity uncertainties are split into a "Luminosity" category which refers to our uncertainty on the inelastic $p\bar{p}$ cross-section, and a "Luminosity Monitor" category, which refers to CDF-specific luminosity uncertainty. The "Luminosity" category, taken to be 3.8% and the "Luminosity Monitor" uncertainty is taken to be 4.4% for all templates of signal and background that are normalized to theoretical predictions times the luminosity measurement. Components that are already normalized to data observations in control samples do not have this uncertainty. This breakdown is necessary for proper correlation with D0's luminosity uncertainty, although is not strictly necessary for the CDF combination presented in this note.

B. Systematic Uncertainties

Systematic uncertainties are incorporated by marginalizing the likelihood function over variations in the uncertain parameters, called "nuisance parameters". Each nuisance parameter is considered to be independent of the others, but each one may have an effect on any of the signal or background predictions in any of the channels. Nuisance parameters included in this combination include the integrated luminosity, the jet energy scale, the b-tag efficiency scale factor, mistag uncertainties, the lepton trigger efficiencies, the lepton identification efficiencies and fake rates, Monte Carlo generator differences, uncertainties due to missing higher-order terms in the signal and background MC predictions, Monte Carlo modeling of ISR, FSR and PDFs, background production cross sections for $t\bar{t}$, diboson, and other backgrounds, mistag matrix uncertainties, the heavy-flavor fraction in W+jets, and the uncertainties in non-W contributions. Full listings of the nuisance parameters affecting these analyses are summarized in Tables III, IV, VII, IX, X, XII, XIV, XVI, XVII, XVIII, XIX, XX, and XXII at the end of this note, and are discussed in more detail in the analysis documentation. The nuisance parameters affect the predicted rates of different signal and background processes, and some nuisance parameters have shape uncertainties associated with them as well.

Rate uncertainties on template histograms are incorporated by multiplying the dependences of each rate on each nuisance parameter.

$$s_{\text{varied}} = s_{\text{central}} \prod_{i=1}^{n_{\text{params}}} (1 + f_i \eta_i) \tag{7}$$

where s_{varied} is the systematically varied normalization scale factor on a particular prediction histogram (signal or background) in a channel, s_{central} is the central-value normalization scale factor for that template, f_i is the relative uncertainty on s due to nuisance parameter i, and η_i is the random truncated-Gaussian-distributed nuisance parameter. Indices for the analysis channel and background or signal source template have been suppressed. The multiplicative technique used here means that the nuisance parameter truncations are all independent of each other.

Shape uncertainties are handled by varying the template shapes according to the nuisance parameters η_i. Systematically-varied shapes are supplied by the analysis teams as histograms which are generated with systematically varied parameters. These parameters may be the same ones as are responsible for the rate variations, and the variations are taken to be correlated. For example, a jet energy scale variation affects both the rate and the shape of most expected signal histograms. All analyses now use histograms of sophisticated multivariate discriminants in order to present their results, and the left-right template shifting interpolation is no longer used to incorporate shape uncertainties. Instead, the simpler method of linearly interpolating between the central value shapes and the systematically varied shapes in each bin according to the value of the nuisance parameter. Shape systematics are compounded by adding linearly the changes due to several shape variations in each bin. Shape systematics are extrapolated beyond the usual $\pm 1\sigma$ variations provided by the analysis teams. If a particular choice of shape variations results in a negative prediction for any signal or background component in any bin, then the prediction for that component is set to zero in that bin, but it does not prevent that variation from being applied to other bins.

Another source of rate and shape variation is limited MC statistics in each bin of the template histograms. Each analysis supplies histograms along with their independent uncertainties in `ROOT` histogram objects. These uncertainties do not include the correlated rate and shape uncertainties described above, but are meant to cover the effects of MC

statistics (or data statistics, if data control regions are used to predict the composition of the selected events in the signal region).

C. Numerical Integration

The space spanned by the nuisance parameters has a very large dimension – there are 79 independent uncertain parameters in all at $m_H = 115$ GeV, and 33 independent uncertain parameters at $m_H = 165$ GeV. The calculation of the posterior integrates over all possible values of the nuisance parameters, weighted by their priors. These priors are truncated Gaussian distributions with unit width (before truncation). The domain of each nuisance parameter is truncated in order to keep the prediction of the rate of each template non-negative; no other truncation is applied. Since analyzers supply $\pm 1\sigma$ uncertainties on rates and shapes, the impacts of multi-sigma variations are extrapolations of the one sigma variations. The factorization and renormalization scale uncertainty on the $gg \to H$ production cross section has also been tested with a flat prior between the low bound and the high bound. The effect on the limit of a box-shaped prior between the low bound and the high bound and a truncated Gaussian where the upper and lower edges of the theory uncertainty are treated as $\pm 1\sigma$ variations is small, about 4%.

Markov chain Monte Carlo integration, using the Metropolis-Hastings algorithm [38], is the algorithm chosen to perform the high-dimensional integrals over the nuisance parameters. This algorithm is commonly used to evaluate high-dimensional integrals such as ours, which occur frequently in Bayesian inference. All integrals start their Markov chains at the point in nuisance parameter space at which all parameters are zero (corresponding to the central values of all predictions). A proposal function determines where to step next in nuisance parameter space, and the Markov chain moves to the proposed point if it has a higher value of the likelihood or if a random number between 0 and 1 is less than the ratio of the likelihood at the new point divided by the likelihood at the old point. The first 500 steps are discarded in the standard "burn-in" procedure. The proposal function is chosen to be a multivariate Gaussian, with an axis along each nuisance parameter. The magnitudes chosen for the axis lengths are chosen by a pre-scan of the likelihood function evaluated varying one parameter at a time centering the other parameters on their central values. The overall scale of the step size is then scaled down by the square root of the number of nuisance parameters, to start off with a reasonable accept/reject ratio. Every 5000 Markov chain steps this accept/reject ratio is recomputed, and an overall scale factor on the Markov chain step size is adjusted upwards (downwards) by a factor of 1.2 if the accept ratio is higher than 0.5 (lower than 0.3). This algorithm focuses on parts of parameter space for which the integrand is largest, which makes it an efficient choice for the integration performed here, and the automatic tuning of the proposal function allows general use on the variety of input channels with no modifications to parameters.

All limits are quoted at the 95% credibility level. Expected limits are computed using a sample of 1000 background-only pseudoexperiments for each mass point of each analysis or combination. On each pseudoexperiment, new values of the nuisance parameters are drawn from the Gaussian distributions specified in the systematic uncertainty tables, and Poisson random pseudodata are drawn from the systematically smeared predictions. In order to reduce the amount of CPU used in the combination and to get more reliable $\pm 2\sigma$ expected limit estimations, the distribution of limits in the pseudoexperiments is fit to the density function $d(R)$:

$$d(R) = p_1 (R - p_2)^{p_3} e^{-p_4 R}, \tag{8}$$

where p_1, p_2, p_3, and p_4 are freely-floating fit parameters. This function is then integrated to obtain the desired quantiles, which correspond to 2.275% of limits being below the -2σ limit expectation in a large ensemble of background-only outcomes, 16% being below the -1σ limit expectation, 50% being below the median expectation, 84% being below the $+1\sigma$ expectation, and 97.725% being below the $+2\sigma$ expectation.

V. INDIVIDUAL CHANNEL LIMITS

In order to validate the input histogram preparation and the combination method, the observed and expected limits have been recomputed for each of the contributing channels before the final combination is performed. The rates and systematic uncertainties of each of the signal contributions and the backgrounds are compared with the available documentation. For the individual channel limits, the same Markov chain integration technique is performed as for the combination, and the numerical precision due to Monte Carlo statistics in the limit calculation and the expected limit calculation is expected to be below 2%. Tables V, VI, VIII, XI, XIII, XV, XXI, and XXIII at the end of this note compare the observed and expected limits computed by the analysis teams and the reproductions computed here. In most cases, the agreement is exquisite; the results are handled in the same way in the combination and by each analysis team. In one case, for the $WH + ZH \to \not{E}_T + b\bar{b}$ channels, the analysis team reports limits before overlapping events with the $WH \to \ell\nu b\bar{b}$ channels have been subtracted, whereas for the combination, this subtraction is included.

VI. COMBINATION RESULTS

The results of the combination are given in Table XXIV, and in Figure 1. Figure 2 shows the observed and expected limits obtained in combination and also those of the individual analyses. The SM Higgs mass limit from LEP [39] is included in the plots. The same procedure for computing the individual channel limits is applied, but a joint likelihood is formed for all channels together, and variations of shared nuisance parameters, which affect both rates and shapes, are all performed with 100% correlations between parameters with the same name, and 0% correlation between parameters with different names.

To visualize the combined results better, the data are collected from all channels and are classified by the signal-to-background ratio in each bin. Bins of nearby s/b are collected together, and plotted vs $\log_{10}(s/b)$ in Figure 3 for $m_H = 110$ and 115 GeV/c^2, and in Figure 4 for $m_H = 150$ and 160 GeV/c^2. The data are then integrated from the high s/b side towards the lower, and the data counts are shown in Figures 3 and 4 for the same four Higgs boson masses. These integrals answer the question of how many events were observed,compared with the signal and background predictions. Because many bins of different s/b are used to make the final limit, there is an arbitrary choice of where to put a cut to answer that question. A drawback of these representations is that systematic uncertainties are not shown.

In order to represent how the signal compares with the posterior uncertainty on the background, and also how the data compare with the background and signal-plus-background predictions, we show in Figure 5 the distribution of data events, again sorted by s/b, with the background fit to the data and then subtracted. The remaining systematic uncertainty on the background after the fit is indicated in the figures, as is the signal prediction. These distributions are shown for $m_H = 115$ and 160 GeV/c^2.

VII. PROJECTIONS

As data are accumulated, the sensitivity of the searches is expected to increase. A naive extrapolation of the sensitivity is to scale the median expected limit with $1/\sqrt{\int Ldt}$. This approximation makes several assumptions: 1) that the background levels in the high s/b bins is sufficiently large that the distribution of data events is expected to be in the Gaussian regime of the Poisson distribution, 2) that the systematic uncertainties scale with $1/\sqrt{\int Ldt}$ for each channel, 3) that the analysis techniques remain constant, 4) that the detector performance remains constant and also does not degrade with increased instantaneous luminosity, and 5) that the tested models do not change. The experience on CDF is that the detector performance remains nearly constant, with only a mild drop due to the increased instantaneous luminosity. Larger control samples allow better constraints on systematic uncertainties, and also can be used to test extrapolations into signal regions by refining the definitions of the control samples. Analysis improvements such as increasing acceptance by exploiting previously unused trigger paths and event topologies, as well as improved separation of signal from background through the use of multivariate techniques and combinations of multivariate techniques have brought about increases in sensitivity that surpass what is expected from the $1/\sqrt{\int Ldt}$ dependence alone. The comparison of the achieved expected limits and the $1/\sqrt{\int Ldt}$ extrapolations is shown in Figure 6 for $m_H = 115$ and 160 GeV/c^2.

In Figure 6, the integrated luminosity at which to place a point is depends on the integrated luminosity used in each contributing channel, as well as the corresponding sensitivity contributed by each channel. For example, if a channel has a large contribution to the sensitivity, the average luminosity should be closer to that channel's luminosity than to a channel which contributes relatively little to the total. The strategy to average the luminosities together is to assume that the median expected limit scales as $1/\sqrt{\int Ldt}$ for an analysis whose technique does not change over time. The sensitivities are computed for each channel at 1 fb^{-1}, and then the combined sensitivity at 1 fb^{-1} is scaled up to the avearage luminosity to match the combined sensitivity obtained with the combination of different-luminosity channels. This procedure results in the following formula to compute the sensitivity-weighted luminosity

$$\langle L \rangle = \frac{\sum_{i=1}^{n_{\rm chans}} \frac{1}{\left(R^i_{\rm exp}\right)^2}}{\sum_{i=1}^{n_{\rm chans}} \frac{1}{\left(R^i_{\rm exp}\right)^2 L_i}}, \tag{9}$$

where L_i is the integrated luminosity analyzed in channel i, and $R^i_{\rm exp}$ is the median expected 95% CL limit on $R = \sigma_H/\sigma_H^{\rm SM}$ for channel i. The production cross sections and branching ratios have been adjusted in the older

analyses to the same values used in the current analysis so that the comparison only shows improvements due to analysis technique and collected data.

The projection figures include estimations of how much the sensitivity could be improved over time as work is done on the analyses. The estimations were made in late 2007, based on the Summer 2007 estimations of sensitivity. A factor of 1.5 in the expected limit was estimated to be attainable with improvements known to exist but not yet in the analyses, and a further factor of 1.5 was estimated from ideas that had yet to be tried. Both of these curves are shown, as the top and bottom edges of light orange bands in the figures. For both the low-mass and high-mass searches, the first factor of 1.5 has already been achieved.

Figure 7 shows the same projections, but the expected limits have all been divided by $\sqrt{2}$ to simulate the effect of combining with D0, assuming performance equal to CDF's. Figure 8 shows the chances of observing a 2σ excess or 3σ evidence as a function of m_H, assuming a Higgs boson is present and the production cross section and decay parameters are as predicted by the SM. CDF and D0 are assumed to contribute equally, and the performance level is shown both for the currently achieved performance level and also for an additional factor of 1.5. Two luminosity scenarios are considered, 5 fb^{-1} and 10 fb^{-1} of analyzed luminosity per experiment. Only the sensitivity estimated by the signal and background templates and their systematic uncertainties is shown in these plots, and no account is taken of the data already observed. In particular, the current Tevatron Higgs combination corresponding to the present CDF combination exludes the region $158 < m_H < 175$ GeV/c^2 [40], and so the chances of observing an excess or evidence are lessened when considering the data that have already been collected. Furthermore, even if a SM Higgs boson is nonetheless assumed to exist in that range, it will take more data and additional luck in order to accumulate enough candidates to amass the evidence after the unlucky downward fluctuation.

VIII. ACKNOWLEDGEMENTS

The authors would like to thank all members of the CDF Higgs Discovery group, particularly those who provided the results for combination.

---

[1] CDF Collaboration, CDF Note 9999 (2009).
[2] E. Arik, O. Cakir, S. A. Cetin and S. Sultansoy, Acta Phys. Polon. B **37**, 2839-2850 (2006). Available online as `arXiv:hep-ph/0502050`.
[3] G. D. Kribs, T. Plehn, M. Spannowsky and T. M. P. Tait, Phys. Rev. D **76**, 075016 (2007).
[4] T. Aaltonen *et al.* The CDF and D0 Collaborations, and the Tevatron New Physics and Higgs Working Group, arXiv:1005.3216 [hep-ex] (2010), submitted to Phys. Rev. D rapid communications.
[5] C. Anastasiou, R. Boughezal and F. Petriello, "Mixed QCD-electroweak corrections to Higgs boson production in gluon fusion", arXiv:0811.3458 [hep-ph] (2008).
[6] D. de Florian and M. Grazzini, "Higgs production through gluon fusion: updated cross sections at the Tevatron and the LHC", arXiv:0901.2427v1 [hep-ph] (2009).
[7] R. V. Harlander and W. B. Kilgore, Phys. Rev. Lett. **88**, 201801 (2002).
[8] C. Anastasiou and K. Melnikov, Nucl. Phys. B **646**, 220 (2002).
[9] V. Ravindran, J. Smith, and W. L. van Neerven, Nucl. Phys. B **665**, 325 (2003).
[10] S. Actis, G. Passarino, C. Sturm, and S. Uccirati, Phys. Lett. B **670**, 12 (2008).
[11] U. Aglietti, R. Bonciani, G. Degrassi, A. Vicini, "Two-loop electroweak corrections to Higgs production in proton-proton collisions", arXiv:hep-ph/0610033v1 (2006).
[12] S. Catani, D. de Florian, M. Grazzini and P. Nason, "Soft-gluon resummation for Higgs boson production at hadron colliders," JHEP **0307**, 028 (2003) [arXiv:hep-ph/0306211].
[13] A. D. Martin, W. J. Stirling, R. S. Thorne and G. Watt, "Parton distributions for the LHC, arXiv:0901.0002 [hep-ph] (2009).
[14] C. Anastasiou, G. Dissertori, M. Grazzini, F. Stöckli and B. R. Webber, arXiv:0905.3529 [hep-ph].
[15] J. Baglio and A. Djouadi, arXiv:1003.4266v1 [hep-ph] (2010). We have obtained extended versions of the table of WH and ZH cross sections for all Higgs boson masses we test, and with more digits of precision, from the authors, before the conference. A newer version is available (but not in time for us to include for our ICHEP 2010 results), in J. Baglio and A. Djouadi, arXiv:1003.4266v2 [hep-ph] (2010), which predicts 4% lower WH and ZH cross sections due to including CKM matrix elements.
[16] K. A. Assamagan *et al.* [Higgs Working Group Collaboration], "The Higgs working group: Summary report 2003," arXiv:hep-ph/0406152.
[17] O. Brein, A. Djouadi, and R. Harlander, Phys. Lett. B **579**, 149 (2004).
[18] M. L. Ciccolini, S. Dittmaier, and M. Kramer, Phys. Rev. D **68**, 073003 (2003).
[19] E. Berger and J. Campbell, Phys. Rev. D **70** 073011 (2004).

[20] T. Sjöstrand, L. Lonnblad and S. Mrenna, arXiv:hep-ph/0108264 (2001);
T. Sjöstrand, P. Eden, C. Friberg, L. Lonnblad, G. Miu, S. Mrenna and E. Norrbin, Comput. Phys. Commun. **135**, 238 (2001). [arXiv:hep-ph/0010017].
[21] H. L. Lai *et al.*, Phys. Rev D **55**, 1280 (1997).
[22] A. Djouadi, K.Kalinowski and M. Spira, Comp. Phys. Commun. **108C** 56 (1998).
[23] CDF Collaboration, CDF Note 10193 (2010).
See also `http://www-cdf.fnal.gov/physics/new/hdg//Results_files/results/whlnubb_jul10/`
[24] D. Acosta *et al.*, (CDF Collaboration), Phys. Rev. D **71**, 052003 (2005).
[25] A. Abulencia *et al.*, (CDF Collaboration), Phys. Rev. D **74**, 072006 (2006).
[26] CDF Collaboration, CDF Note 10217 (2010).
[27] CDF Collaboration, CDF Note 10221 (2010).
[28] CDF Collaboration, CDF Note 10235 (2010). For a combination of the CMIO and mainline $ZH \to \ell^+\ell^- b\bar{b}$ channels, see `http://www-cdf.fnal.gov/physics/new/hdg//Results_files/results/zhllbb_jul10/comb/zhllbb_comb_web/`.
[29] CDF Collaboration, CDF Note 10065 (2010).
[30] CDF Collaboration, CDF Note 10212 (2010).
[31] CDF Collaboration, CDF Note 9891 (2009).
[32] M.L. Mangano, M. Moretti, F. Piccinini, R. Pittau, A. Polosa, JHEP 0307:001; hep-ph/0206293 (2003).
[33] The CDF and D0 Collaborations and the Tevatron Electroweak Working Group, arXiv:0903.2503 [hep-ex].
[34] S. Moch and P. Uwer, Nucl. Phys. Proc. Suppl. **183**, 75 (2008) [arXiv:0807.2794 [hep-ph]];
N. Kidonakis and R. Vogt, Phys. Rev. D **78**, 074005 (2008) [arXiv:0805.3844 [hep-ph]].
[35] N. Kidonakis, Phys. Rev. D **74**, 114012 (2006) [arXiv:hep-ph/0609287].
[36] J.M. Campbell, R.K. Ellis, Phys. Rev. D62:114012 (2000), hep-ph/0006304. See also `http://mcfm.fnal.gov/index.html`.
[37] J. Campbell and R. K. Ellis, Phys. Rev. D **65**, 113007 (2002).
[38] N. Metropolis, A.W. Rosenbluth, M.N. Rosenbluth, A.H. Teller, and E. Teller. "Equations of State Calculations by Fast Computing Machines". *Journal of Chemical Physics*, 21(6):1087-1092, (1953).
W.K. Hastings. "Monte Carlo Sampling Methods Using Markov Chains and Their Applications", *Biometrika*, 57(1):97-109, (1970).
[39] The ALEPH, DELPHI, L3 and OPAL Collaborations, and the LEP Higgs Working Group, Phys. Lett. B **565**, 61 (2003).
[40] The CDF and D0 Collaborations, and the Tevatron New Phenomena and Higgs Working Group, "Combined CDF and D0 Upper Limits on Standard Model Higgs-Boson Production with up to 6.7 fb^{-1} of Data", FERMILAB-CONF-10-257-E, CDF Note 10241, D0 Note 6096 (2010).
[41] CDF Collaboration, CDF Note 10133 (2010).
[42] CDF Collaboration, CDF Note 10010 (2010).
[43] CDF Collaboration, CDF Note 10232 (2010).
[44] CDF Collaboration, CDF Note 10226 (2010).

TABLE I: Analyzed integrated luminosities and references for the main CDF SM Higgs search channels combined in this note

Channel	$\int \mathcal{L}dt$ (fb^{-1})	Reference
$WH \to \ell\nu b\bar{b}$ (triggered leptons+isotrk) (NN) (2-Jets)	5.7	[23]
$WH \to \ell\nu b\bar{b}$ (triggered leptons+extened muons) (ME) (3-Jets)	5.6	[26]
$WH + ZH \to \not\!\!E_T + b\bar{b}$	5.7	[30]
$ZH \to \ell^+\ell^- b\bar{b}$	5.7	[27, 28]
$H \to \tau^+\tau^-$	2.3	[41]
$WH + ZH \to jjb\bar{b}$	4.0	[42]
$H \to \gamma\gamma$	5.4	[29]
$H \to W^+W^- \to \ell^+\nu_l\ell'^-\bar{\nu}_{\ell'}$	5.9	[43, 44]

TABLE II: The production cross sections and decay branching fractions for the SM Higgs boson assumed for the combination.

m_H (GeV/c^2)	$\sigma_{gg\to H}$ (fb)	σ_{WH} (fb)	σ_{ZH} (fb)	σ_{VBF} (fb)	$\sigma_{t\bar{t}H}$ (fb)	$B(H\to b\bar{b})$ (%)	$B(H\to c\bar{c})$ (%)	$B(H\to\tau^+\tau^-)$ (%)	$B(H\to W^+W^-)$ (%)	$B(H\to ZZ)$ (%)	$B(H\to\gamma\gamma)$ (%)
100	1861	291.9	169.8	99.5	8.000	80.33	3.542	7.920	1.052	0.1071	0.1505
105	1618	248.4	145.9	93.3	7.062	78.57	3.463	7.821	2.307	0.2035	0.1689
110	1413	212.0	125.7	87.1	6.233	75.90	3.343	7.622	4.585	0.4160	0.1870
115	1240	181.9	108.9	79.07	5.502	71.95	3.169	7.288	8.268	0.8298	0.2029
120	1093	156.4	94.4	71.65	4.857	66.49	2.927	6.789	13.64	1.527	0.2148
125	967	135.1	82.3	67.37	4.279	59.48	2.617	6.120	20.78	2.549	0.2204
130	858	116.9	71.9	62.5	3.769	51.18	2.252	5.305	29.43	3.858	0.2182
135	764	101.5	63.0	57.65	3.320	42.15	1.854	4.400	39.10	5.319	0.2077
140	682	88.3	55.3	52.59	2.925	33.04	1.453	3.472	49.16	6.715	0.1897
145	611	77.0	48.7	49.15	2.593	24.45	1.075	2.585	59.15	7.771	0.1653
150	548	67.3	42.9	45.67	2.298	16.71	0.7345	1.778	68.91	8.143	0.1357
155	492	58.9	37.9	42.19	2.037	9.88	0.4341	1.057	78.92	7.297	0.09997
160	439	50.8	33.1	38.59	1.806	3.74	0.1646	0.403	90.48	4.185	0.05365
165	389	44.6	30.0	36.09	1.607	1.29	0.05667	0.140	95.91	2.216	0.02330
170	349	40.2	26.6	33.58	1.430	0.854	0.03753	0.093	96.39	2.351	0.01598
175	314	35.6	23.7	31.11	1.272	0.663	0.02910	0.073	95.81	3.204	0.01236
180	283	31.4	21.1	28.57	1.132	0.535	0.02349	0.059	93.25	5.937	0.01024
185	255	28.2	18.9	26.81	1.004	0.415	0.01823	0.046	84.50	14.86	0.008128
190	231	25.1	17.0	24.88	0.890	0.340	0.01490	0.038	78.70	20.77	0.006774
195	210	22.4	15.3	23	0.789	0.292	0.01281	0.033	75.88	23.66	0.005919
200	192	20.0	13.7	21.19	0.700	0.257	0.01128	0.029	74.26	25.33	0.005285

TABLE III: Systematic uncertainties on the signal and background contributions for the $WH \to \ell\nu b\bar{b}$ tight double tag (TDT), loose double tag (LDT), looser double tag (LDTX), and single tag (ST) 2 jet channels. Systematic uncertainties are listed by name; see the original references for a detailed explanation of their meaning and on how they are derived. Systematic uncertainties for WH shown in this table are obtained for $m_H = 115$ GeV/c^2. Uncertainties are relative, in percent, and are symmetric unless otherwise indicated.

CDF: tight and loose double-tag (TDT and LDT) $WH \to \ell\nu b\bar{b}$ channel relative uncertainties (%)

Contribution	W+HF	Mistags	Top	Diboson	Non-W	WH
Luminosity ($\sigma_{\rm inel}(p\bar{p})$)	0	0	3.8	3.8	0	3.8
Luminosity Monitor	0	0	4.4	4.4	0	4.4
Lepton ID	0	0	2	2	0	2
Jet Energy Scale	0	0	0	0	0	2
Mistag Rate	0	35	0	0	0	0
B-Tag Efficiency	0	0	8.6	8.6	0	8.6
$t\bar{t}$ Cross Section	0	0	10	0	0	0
Diboson Rate	0	0	0	11.5	0	0
Signal Cross Section	0	0	0	0	0	5
HF Fraction in W+jets	45	0	0	0	0	0
ISR+FSR+PDF	0	0	0	0	0	5
QCD Rate	0	0	0	0	40	0

CDF: looser double-tag (LDTX) $WH \to \ell\nu b\bar{b}$ channel relative uncertainties (%)

Contribution	W+HF	Mistags	Top	Diboson	Non-W	WH
Luminosity ($\sigma_{\rm inel}(p\bar{p})$)	0	0	3.8	3.8	0	3.8
Luminosity Monitor	0	0	4.4	4.4	0	4.4
Lepton ID	0	0	2	2	0	2
Jet Energy Scale	0	0	0	0	0	2.2
Mistag Rate	0	36	0	0	0	0
B-Tag Efficiency	0	0	13.6	13.6	0	13.6
$t\bar{t}$ Cross Section	0	0	10	0	0	0
Diboson Rate	0	0	0	11.5	0	0
Signal Cross Section	0	0	0	0	0	5
HF Fraction in W+jets	45	0	0	0	0	0
ISR+FSR+PDF	0	0	0	0	0	7.7
QCD Rate	0	0	0	0	40	0

CDF: single tag (ST) $WH \to \ell\nu b\bar{b}$ channel relative uncertainties (%)

Contribution	W+HF	Mistags	Top	Diboson	Non-W	WH
Luminosity ($\sigma_{\rm inel}(p\bar{p})$)	0	0	3.8	3.8	0	3.8
Luminosity Monitor	0	0	4.4	4.4	0	4.4
Lepton ID	0	0	2	2	0	2
Jet Energy Scale	0	0	0	0	0	2
Mistag Rate	0	35	0	0	0	0
B-Tag Efficiency	0	0	4.3	4.3	0	4.3
$t\bar{t}$ Cross Section	0	0	10	0	0	0
Diboson Rate	0	0	0	11.5	0	0
Signal Cross Section	0	0	0	0	0	5
HF Fraction in W+jets	42	0	0	0	0	0
ISR+FSR+PDF	0	0	0	0	0	3.0
QCD Rate	0	0	0	0	40	0

TABLE IV: Systematic uncertainties on the signal and background contributions for the $WH \to \ell\nu b\bar{b}$ tight double tag (TDT), loose double tag (LDT), and single tag (ST) 3 jet channels. Systematic uncertainties are listed by name; see the original references for a detailed explanation of their meaning and on how they are derived. Systematic uncertainties for WH shown in this table are obtained for $m_H = 115$ GeV/c^2. Uncertainties are relative, in percent, and are symmetric unless otherwise indicated.

CDF: tight and loose double-tag (TDT and LDT) $WH \to \ell\nu b\bar{b}$ channel relative uncertainties (%)

Contribution	W+HF	Mistags	Top	Diboson	Non-W	WH
Luminosity ($\sigma_{\rm inel}(p\bar{p})$)	0	0	3.8	3.8	0	3.8
Luminosity Monitor	0	0	4.4	4.4	0	4.4
Lepton ID	0	0	2	2	0	2
Jet Energy Scale	0	0	0	0	0	13.5
Mistag Rate	0	9	0	0	0	0
B-Tag Efficiency	0	0	8.4	8.4	0	8.4
$t\bar{t}$ Cross Section	0	0	10	0	0	0
Diboson Rate	0	0	0	10	0	0
Signal Cross Section	0	0	0	0	0	10
HF Fraction in W+jets	30	0	0	0	0	0
ISR+FSR+PDF	0	0	0	0	0	21.4
QCD Rate	0	0	0	0	40	0

CDF: single tag (ST) $WH \to \ell\nu b\bar{b}$ channel relative uncertainties (%)

Contribution	W+HF	Mistags	Top	Diboson	Non-W	WH
Luminosity ($\sigma_{\rm inel}(p\bar{p})$)	0	0	3.8	3.8	0	3.8
Luminosity Monitor	0	0	4.4	4.4	0	4.4
Lepton ID	0	0	2	2	0	2
Jet Energy Scale	0	0	0	0	0	15.8
Mistag Rate	0	13.3	0	0	0	0
B-Tag Efficiency	0	0	3.5	3.5	0	3.5
$t\bar{t}$ Cross Section	0	0	10	0	0	0
Diboson Rate	0	0	0	10	0	0
Signal Cross Section	0	0	0	0	0	10
HF Fraction in W+jets	30	0	0	0	0	0
ISR+FSR+PDF	0	0	0	0	0	13.1
QCD Rate	0	0	0	0	40	0

TABLE V: Observed and expected limits for the twelve total $WH \to \ell\nu b\bar{b}$ 2-jet neural network channels. Also listed are the limits from [23]. The limits are all given in units of $R = \sigma/\sigma_{SM}$, assuming SM branching fractions.

m_H (GeV/c^2)	Observed limit/SM	median expected	CDF 10193 observed	CDF 10193 expected
100	2.03	2.35	1.98	2.34
105	3.07	2.60	3.02	2.68
110	3.82	2.95	3.74	2.94
115	4.54	3.37	4.47	3.48
120	5.43	4.12	5.25	4.07
125	6.38	4.79	6.26	4.99
130	9.09	6.27	8.87	6.29
135	12.70	8.54	12.5	8.54
140	15.77	12.36	15.8	12.2
145	25.24	17.83	25.3	17.9
150	44.15		44.3	28.2

TABLE VI: Observed and expected limits for the twelve total $WH \to \ell\nu b\bar{b}$ 3-jet matrix element channels. Also listed are the limits from [26]. The limits are all given in units of $R = \sigma/\sigma_{SM}$, assuming SM branching fractions.

m_H (GeV/c^2)	Observed limit/SM	median expected	CDF 10217 observed	CDF 10217 expected
100	4.92	12.01	5.1	12.2
105	6.27	12.89	5.6	12.9
110	8.71	13.87	8.6	13.9
115	8.64	15.13	8.5	15.8
120	11.15	19.61	10.8	19.5
125	12.15	22.94	12.4	23.0
130	17.07	29.03	17.3	28.1
135	24.00	40.74	22.9	39.5
140	34.38	54.93	33.7	56.1
145	43.93	79.22	42.5	77.9
150	83.33	123.12	80.5	119.8

TABLE VII: Systematic uncertainties on the signal and background contributions for the $WH, ZH \to \not\!\!E_T b\bar{b}$ tight double tag (TDT), loose double tag (LDT), and single tag (ST) channels. Systematic uncertainties are listed by name; see the original references for a detailed explanation of their meaning and on how they are derived. Systematic uncertainties for ZH and WH shown in this table are obtained for $m_H = 120$ GeV/c^2. Uncertainties are relative, in percent, and are symmetric unless otherwise indicated.

Tight double-tag (TDT) $WH, ZH \to \not\!\!E_T b\bar{b}$ channel relative uncertainties (%)

Contribution	ZH	WH	Multijet	Top Pair	S. Top	Di-boson	W + h.f.	Z + h.f.
Luminosity	3.8	3.8		3.8	3.8	3.8	3.8	3.8
Lumi Monitor	4.4	4.4		4.4	4.4	4.4	4.4	4.4
Tagging SF	10.4	10.4		10.4	10.4	10.4	10.4	10.4
Trigger Eff. (shape)	1.0	1.2	1.1	0.7	1.1	1.6	1.7	1.3
Lepton Veto	2.0	2.0		2.0	2.0	2.0	2.0	2.0
PDF Acceptance	2.0	2.0		2.0	2.0	2.0	2.0	2.0
JES (shape)	$^{+3.0}_{-3.0}$	$^{+3.5}_{-4.7}$	$^{-4.0}_{+3.8}$	$^{+1.1}_{-1.1}$	$^{+2.4}_{-4.7}$	$^{+8.2}_{-6.1}$	$^{+7.3}_{-11.8}$	$^{+6.5}_{-8.3}$
ISR	$^{+4.4}_{+3.7}$							
FSR	$^{+1.8}_{+4.4}$							
Cross-Section	5	5		10	10	6	30	30
Multijet Norm. (shape)			22					

Loose double-tag (LDT) $WH, ZH \to \not\!\!E_T b\bar{b}$ channel relative uncertainties (%)

Contribution	ZH	WH	Multijet	Top Pair	S. Top	Di-boson	W + h.f.	Z + h.f.
Luminosity	3.8	3.8		3.8	3.8	3.8	3.8	3.8
Lumi Monitor	4.4	4.4		4.4	4.4	4.4	4.4	4.4
Tagging SF	11.6	11.6		11.6	11.6	11.6	11.6	11.6
Trigger Eff. (shape)	1.2	1.3	1.1	0.7	1.2	1.2	1.8	1.3
Lepton Veto	2.0	2.0		2.0	2.0	2.0	2.0	2.0
PDF Acceptance	2.0	2.0		2.0	2.0	2.0	2.0	2.0
JES (shape)	$^{+3.7}_{-3.7}$	$^{+4.0}_{-4.0}$	$^{-5.4}_{+5.2}$	$^{+1.1}_{-0.7}$	$^{+4.2}_{-4.2}$	$^{+7.0}_{-7.0}$	$^{+1.3}_{-7.6}$	$^{+6.2}_{-7.1}$
ISR	$^{+1.4}_{-2.9}$							
FSR	$^{+5.3}_{+2.5}$							
Cross-Section	5.0	5.0		10	10	6	30	30
Multijet Norm. (shape)			11					

Single-tag (ST) $WH, ZH \to \not\!\!E_T b\bar{b}$ channel relative uncertainties (%)

Contribution	ZH	WH	Multijet	Top Pair	S. Top	Di-boson	W + h.f.	Z + h.f.
Luminosity	3.8	3.8		3.8	3.8	3.8	3.8	3.8
Lumi Monitor	4.4	4.4		4.4	4.4	4.4	4.4	4.4
Tagging SF	5.2	5.2		5.2	5.2	5.2	5.2	5.2
Trigger Eff. (shape)	0.9	1.1	1.1	0.7	1.1	1.3	2.0	1.4
Lepton Veto	2.0	2.0		2.0	2.0	2.0	2.0	2.0
PDF Acceptance	2.0	2.0		2.0	2.0	2.0	2.0	2.0
JES (shape)	$^{+3.8}_{-3.8}$	$^{+3.8}_{-3.8}$	$^{-5.2}_{+5.6}$	$^{+0.7}_{-0.8}$	$^{+4.6}_{-4.6}$	$^{+7.0}_{-5.6}$	$^{+12.4}_{-12.7}$	$^{+8.3}_{-8.1}$
ISR	$^{-1.0}_{-1.5}$							
FSR	$^{+2.0}_{-0.1}$							
Cross-Section	5.0	5.0		10	10	6	30	30
Multijet Norm. (shape)			10					

TABLE VIII: Observed and expected limits for the $WH + ZH \rightarrow \not\!\!E_T + b\bar{b}$ channels, with the single-tag and double-tag analyses combined. The observed and median expected limits computed with the Markov chain method are listed. Also listed are the limits from [30]. The limits are all given in units of $R = \sigma/\sigma_{SM}$, assuming SM branching fractions. The comparison is not perfect, owing to the fact that the limits computed here use the versions of the channels that have the overlap with the $WH \rightarrow \ell\nu b\bar{b}$ channels removed, while the limits in [30] do not have the overlap removed.

m_H (GeV/c^2)	Observed limit/SM	median expected	CDF 10212 observed	CDF 10212 expected
100	2.48	3.27	2.3	3.1
105	2.37	3.42	2.2	3.2
110	2.48	3.72	2.3	3.5
115	2.40	4.20	2.3	4.0
120	2.89	4.96	2.8	4.8
125	3.94	5.78	3.8	5.4
130	4.88	7.10	4.7	6.7
135	5.38	9.50	5.4	9.3
140	7.05	12.47	7.0	11.9
145	9.98	19.09	10.4	18.0
150	19.28	34.55	19.4	32.5

TABLE IX: Systematic uncertainties on the signal and background contributions for the $ZH \to \ell^+\ell^- b\bar{b}$ single tag (ST), tight double tag (TDT), and loose double tag (LDT) channels. The channels are further divided into low and high s/b categories. Systematic uncertainties are listed by name; see the original references for a detailed explanation of their meaning and on how they are derived. Systematic uncertainties for ZH shown in this table are obtained for $m_H = 115$ GeV/c^2. Uncertainties are relative, in percent, and are symmetric unless otherwise indicated.

Single tag (ST) high s/b $ZH \to \ell\ell b\bar{b}$ channel relative uncertainties (%)

Contribution	Fakes	Top	WZ	ZZ	$Z+b\bar{b}$	$Z+c\bar{c}$	Z+mistag	ZH
Luminosity ($\sigma_{\rm inel}(p\bar{p})$)	0	3.8	3.8	3.8	3.8	3.8	0	3.8
Luminosity Monitor	0	4.4	4.4	4.4	4.4	4.4	0	4.4
Lepton ID	0	1	1	1	1	1	0	1
Lepton Energy Scale	0	1.5	1.5	1.5	1.5	1.5	0	1.5
ZH Cross Section	0	0	0	0	0	0	0	5
Fake Leptons	50	0	0	0	0	0	0	0
Jet Energy Scale (shape dep.)	0	$^{+2.0}_{-2.2}$	$^{+3.1}_{-4.7}$	$^{+3.5}_{-5.1}$	$^{+10.6}_{-9.6}$	$^{+9.5}_{-9.4}$	0	$^{+2.2}_{-2.6}$
Mistag Rate (shape dep.)	0	0	0	0	0	0	$^{+14.7}_{-14.8}$	0
B-Tag Efficiency	0	4	4	4	4	4	0	4
$t\bar{t}$ Cross Section	0	10	0	0	0	0	0	0
Diboson Cross Section	0	0	6	6	0	0	0	0
$\sigma(p\bar{p} \to Z+HF)$	0	0	0	0	40	40	0	0
ISR (shape dep.)	0	0	0	0	0	0	0	$^{-4.1}_{-4.8}$
FSR (shape dep.)	0	0	0	0	0	0	0	$^{-1.2}_{-2.4}$

Single tag (ST) low s/b $ZH \to \ell\ell b\bar{b}$ channel relative uncertainties (%)

Contribution	Fakes	Top	WZ	ZZ	$Z+b\bar{b}$	$Z+c\bar{c}$	Z+mistag	ZH
Luminosity ($\sigma_{\rm inel}(p\bar{p})$)	0	3.8	3.8	3.8	3.8	3.8	0	3.8
Luminosity Monitor	0	4.4	4.4	4.4	4.4	4.4	0	4.4
Lepton ID	0	1	1	1	1	1	0	1
Lepton Energy Scale	0	1.5	1.5	1.5	1.5	1.5	0	1.5
ZH Cross Section	0	0	0	0	0	0	0	5
Fake Leptons	50	0	0	0	0	0	0	0
Jet Energy Scale (shape dep.)	0	$^{+1.8}_{-1.6}$	$^{+6.8}_{-4.7}$	$^{+2.9}_{-6.2}$	$^{+11.6}_{-10.2}$	$^{+10.0}_{-10.3}$	0	$^{+3.9}_{-1.4}$
Mistag Rate (shape dep.)	0	0	0	0	0	0	$^{+14.8}_{-14.9}$	0
B-Tag Efficiency	0	4	4	4	4	4	0	4
$t\bar{t}$ Cross Section	0	10	0	0	0	0	0	0
Diboson Cross Section	0	0	6	6	0	0	0	0
$\sigma(p\bar{p} \to Z+HF)$	0	0	0	0	40	40	0	0
ISR (shape dep.)	0	0	0	0	0	0	0	$^{+7.4}_{-2.5}$
FSR (shape dep.)	0	0	0	0	0	0	0	$^{+6.9}_{+1.9}$

Tight double tag (TDT) high s/b $ZH \to \ell\ell b\bar{b}$ channel relative uncertainties (%)

Contribution	Fakes	Top	WZ	ZZ	$Z+b\bar{b}$	$Z+c\bar{c}$	Z+mistag	ZH
Luminosity ($\sigma_{\rm inel}(p\bar{p})$)	0	3.8	3.8	3.8	3.8	3.8	0	3.8
Luminosity Monitor	0	4.4	4.4	4.4	4.4	4.4	0	4.4
Lepton ID	0	1	1	1	1	1	0	1
Lepton Energy Scale	0	1.5	1.5	1.5	1.5	1.5	0	1.5
ZH Cross Section	0	0	0	0	0	0	0	5
Fake Leptons	50	0	0	0	0	0	0	0
Jet Energy Scale (shape dep.)	0	$^{+1.5}_{-1.1}$	$^{+0.0}_{-0.0}$	$^{+1.8}_{-2.7}$	$^{+5.9}_{-6.9}$	$^{+6.0}_{-6.0}$	0	$^{+1.6}_{-0.3}$
Mistag Rate (shape dep.)	0	0	0	0	0	0	$^{+30.9}_{-26.8}$	0
B-Tag Efficiency	0	8	8	8	8	8	0	8
$t\bar{t}$ Cross Section	0	10	0	0	0	0	0	0
Diboson Cross Section	0	0	6	6	0	0	0	0
$\sigma(p\bar{p} \to Z+HF)$	0	0	0	0	40	40	0	0
ISR (shape dep.)	0	0	0	0	0	0	0	$^{-2.1}_{+0.4}$
FSR (shape dep.)	0	0	0	0	0	0	0	$^{-1.7}_{-0.7}$

Tight double tag (TDT) low s/b $ZH \to \ell\ell b\bar{b}$ channel relative uncertainties (%)

Contribution	Fakes	Top	WZ	ZZ	$Z+b\bar{b}$	$Z+c\bar{c}$	Z+mistag	ZH
Luminosity ($\sigma_{\rm inel}(p\bar{p})$)	0	3.8	3.8	3.8	3.8	3.8	0	3.8
Luminosity Monitor	0	4.4	4.4	4.4	4.4	4.4	0	4.4
Lepton ID	0	1	1	1	1	1	0	1
Lepton Energy Scale	0	1.5	1.5	1.5	1.5	1.5	0	1.5
ZH Cross Section	0	0	0	0	0	0	0	5
Fake Leptons	50	0	0	0	0	0	0	0
Jet Energy Scale (shape dep.)	0	$^{+0.5}_{-0.9}$	$^{+0.0}_{-0.0}$	$^{+0.0}_{-3.3}$	$^{+5.7}_{-6.2}$	$^{+7.2}_{-5.6}$	0	$^{+1.5}_{-0.6}$
Mistag Rate (shape dep.)	0	0	0	0	0	0	$^{+31.5}_{-27.2}$	0
B-Tag Efficiency	0	8	8	8	8	8	0	8
$t\bar{t}$ Cross Section	0	10	0	0	0	0	0	0
Diboson Cross Section	0	0	6	6	0	0	0	0
$\sigma(p\bar{p} \to Z+HF)$	0	0	0	0	40	40	0	0
ISR (shape dep.)	0	0	0	0	0	0	0	$^{-1.0}_{-2.7}$
FSR (shape dep.)	0	0	0	0	0	0	0	$^{-5.3}_{-2.8}$

Loose double tag (LDT) high S/B $ZH \to \ell\ell b\bar{b}$ channel relative uncertainties (%)

Contribution	Fakes	Top	WZ	ZZ	$Z+b\bar{b}$	$Z+c\bar{c}$	Z+mistag	ZH
Luminosity ($\sigma_{\rm inel}(p\bar{p})$)	0	3.8	3.8	3.8	3.8	3.8	0	3.8
Luminosity Monitor	0	4.4	4.4	4.4	4.4	4.4	0	4.4
Lepton ID	0			1	1	1	0	1
Lepton Energy Scale	0	1.5	1.5	1.5	1.5	1.5	0	1.5
ZH Cross Section	0	0	0	0	0	0	0	5
Fake Leptons	50	0	0	0	0	0	0	0
Jet Energy Scale (shape dep.)	0	$^{+1.3}_{-0.6}$	$^{+3.2}_{-4.3}$	$^{+3.2}_{-3.0}$	$^{+7.4}_{-7.3}$	$^{+6.3}_{-6.0}$	0	$^{+1.04}_{-0.6}$
Mistag Rate (shape dep.)	0	0	0	0	0	0	$^{+32.1}_{-25.7}$	0
B-Tag Efficiency	0	11	11	11	11	11	0	11
$t\bar{t}$ Cross Section	0	10	0	0	0	0	0	0
Diboson Cross Section	0	0	6	6	0	0	0	0
$\sigma(p\bar{p} \to Z+HF)$	0	0	0	0	40	40	0	0
ISR (shape dep.)	0	0	0	0	0	0	0	$^{+1.4}_{-0.6}$
FSR (shape dep.)	0	0	0	0	0	0	0	$^{+0.4}_{-2.0}$

Loose double tag (LDT) low S/B $ZH \to \ell\ell b\bar{b}$ channel relative uncertainties (%)

Contribution	Fakes	Top	WZ	ZZ	$Z+b\bar{b}$	$Z+c\bar{c}$	Z+mistag	ZH
Luminosity ($\sigma_{\rm inel}(p\bar{p})$)	0	3.8	3.8	3.8	3.8	3.8	0	3.8
Luminosity Monitor	0	4.4	4.4	4.4	4.4	4.4	0	4.4
Lepton ID	0			1	1	1	0	1
Lepton Energy Scale	0	1.5	1.5	1.5	1.5	1.5	0	1.5
ZH Cross Section	0	0	0	0	0	0	0	5
Fake Leptons	50	0	0	0	0	0	0	0
Jet Energy Scale (shape dep.)	0	$^{+1.7}_{-0.2}$	$^{-0.0}_{-3.4}$	$^{+3.1}_{-1.0}$	$^{+8.2}_{-8.6}$	$^{+8.0}_{-8.8}$	0	$^{+0.3}_{-1.8}$
Mistag Rate (shape dep.)	0	0	0	0	0	0	$^{+31.7}_{-26.0}$	0
B-Tag Efficiency	0	11	11	11	11	11	0	11
$t\bar{t}$ Cross Section	0	10	0	0	0	0	0	0
Diboson Cross Section	0	0	6	6	0	0	0	0
$\sigma(p\bar{p} \to Z+HF)$	0	0	0	0	40	40	0	0
ISR (shape dep.)	0	0	0	0	0	0	0	$^{+1.8}_{+5.3}$
FSR (shape dep.)	0	0	0	0	0	0	0	$^{+23.0}_{+7.9}$

TABLE X: Systematic uncertainties on the signal and background contributions for the $ZH \to \ell^+\ell^- b\bar{b}$ single tag (ST), loose double tag (LDT), and tight double tag (TDT) loose muon channels. The channels are further divided to separate events collected from either the muon or missing E_T trigger path. Systematic uncertainties are listed by name; see the original references for a detailed explanation of their meaning and on how they are derived. Systematic uncertainties for ZH shown in this table are obtained for $m_H = 115$ GeV/c^2. Uncertainties are relative, in percent, and are symmetric unless otherwise indicated.

Single tag (ST) loose muons (muon trigger) $ZH \to \ell\ell b\bar{b}$ channel relative uncertainties (%)

Contribution	Fakes	Top	WZ	ZZ	$Z+b\bar{b}$	$Z+c\bar{c}$	Z+mistag	ZH
Luminosity ($\sigma_{\rm inel}(p\bar{p})$)	0	3.8	3.8	3.8	3.8	3.8	0	3.8
Luminosity Monitor	0	4.4	4.4	4.4	4.4	4.4	0	4.4
Lepton ID	0	1	1	1	1	1	0	1
Lepton Energy Scale	0	1.5	1.5	1.5	1.5	1.5	0	1.5
ZH Cross Section	0	0	0	0	0	0	0	5
Fake Leptons	50	0	0	0	0	0	0	0
Jet Energy Scale (shape dep.)	0	$^{+0.01}_{-0.01}$	$^{+0.0}_{-1.3}$	$^{+1.3}_{-2.1}$	$^{+2.9}_{-2.8}$	$^{+3.2}_{-2.3}$	0	$^{+0.2}_{-0.3}$
Mistag Rate (shape dep.)	0	0	0	0	0	0	$^{+14.3}_{-14.4}$	0
B-Tag Efficiency	0	4	4	4	4	4	0	4
$t\bar{t}$ Cross Section	0	10	0	0	0	0	0	0
Diboson Cross Section	0	0	6	6	0	0	0	0
$\sigma(p\bar{p} \to Z + HF)$	0	0	0	0	40	40	0	0
ISR/FSR	0	0	0	0	0	0	0	5
NN Trigger Model	0	5	5	5	5	5	0	5

Loose double tag (LDT) loose muons (muon trigger) $ZH \to \ell\ell b\bar{b}$ channel relative uncertainties (%)

Contribution	Fakes	Top	WZ	ZZ	$Z+b\bar{b}$	$Z+c\bar{c}$	Z+mistag	ZH
Luminosity ($\sigma_{\rm inel}(p\bar{p})$)	0	3.8	3.8	3.8	3.8	3.8	0	3.8
Luminosity Monitor	0	4.4	4.4	4.4	4.4	4.4	0	4.4
Lepton ID	0	1	1	1	1	1	0	1
Lepton Energy Scale	0	1.5	1.5	1.5	1.5	1.5	0	1.5
ZH Cross Section	0	0	0	0	0	0	0	5
Fake Leptons	50	0	0	0	0	0	0	0
Jet Energy Scale (shape dep.)	0	$^{+0.1}_{-0.9}$	$^{+0.0}_{-0.0}$	$^{+0.0}_{-0.0}$	$^{+3.7}_{-4.2}$	$^{+4.0}_{-1.6}$	0	$^{+0.1}_{-0.0}$
Mistag Rate (shape dep.)	0	0	0	0	0	0	$^{+33.6}_{-26.2}$	0
B-Tag Efficiency	0	11	11	11	11	11	0	11
$t\bar{t}$ Cross Section	0	10	0	0	0	0	0	0
Diboson Cross Section	0	0	6	6	0	0	0	0
$\sigma(p\bar{p} \to Z + HF)$	0	0	0	0	40	40	0	0
ISR/FSR	0	0	0	0	0	0	0	3
NN Trigger Model	0	5	5	5	5	5	0	5

Tight double tag (TDT) loose muons (muon trigger) $ZH \to \ell\ell b\bar{b}$ channel relative uncertainties (%)

Contribution	Fakes	Top	WZ	ZZ	$Z+b\bar{b}$	$Z+c\bar{c}$	Z+mistag	ZH
Luminosity ($\sigma_{\rm inel}(p\bar{p})$)	0	3.8	3.8	3.8	3.8	3.8	0	3.8
Luminosity Monitor	0	4.4	4.4	4.4	4.4	4.4	0	4.4
Lepton ID	0	1	1	1	1	1	0	1
Lepton Energy Scale	0	1.5	1.5	1.5	1.5	1.5	0	1.5
ZH Cross Section	0	0	0	0	0	0	0	5
Fake Leptons	50	0	0	0	0	0	0	0
Jet Energy Scale (shape dep.)	0	$^{+1.2}_{-0.0}$	$^{+0.0}_{-0.0}$	$^{+0.0}_{-0.0}$	$^{+2.1}_{-3.3}$	$^{+1.3}_{-0.0}$	0	$^{+0.0}_{-0.0}$
Mistag Rate (shape dep.)	0	0	0	0	0	0	$^{+30.7}_{-26.6}$	0
B-Tag Efficiency	0	8	8	8	8	8	0	8
$t\bar{t}$ Cross Section	0	10	0	0	0	0	0	0
Diboson Cross Section	0	0	6	6	0	0	0	0
$\sigma(p\bar{p} \to Z + HF)$	0	0	0	0	40	40	0	0
ISR/FSR	0	0	0	0	0	0	0	1
NN Trigger Model	0	5	5	5	5	5	0	5

Single tag (ST) loose muons (missing E_T trigger) $ZH \to \ell\ell b\bar{b}$ channel relative uncertainties (%)

Contribution	Fakes	Top	WZ	ZZ	$Z+b\bar{b}$	$Z+c\bar{c}$	Z+mistag	ZH
Luminosity ($\sigma_{\rm inel}(p\bar{p})$)	0	3.8	3.8	3.8	3.8	3.8	0	3.8
Luminosity Monitor	0	4.4	4.4	4.4	4.4	4.4	0	4.4
Lepton ID	0	1	1	1	1	1	0	1
Lepton Energy Scale	0	1.5	1.5	1.5	1.5	1.5	0	1.5
ZH Cross Section	0	0	0	0	0	0	0	5
Fake Leptons	50	0	0	0	0	0	0	0
Jet Energy Scale (shape dep.)	0	$^{+0.0}_{-0.1}$	$^{+0.0}_{-0.0}$	$^{+0.6}_{-0.4}$	$^{+0.6}_{-0.7}$	$^{+0.7}_{-1.0}$	0	$^{+0.0}_{-0.2}$
Mistag Rate (shape dep.)	0	0	0	0	0	0	$^{+14.1}_{-14.1}$	0
B-Tag Efficiency	0	4	4	4	4	4	0	4
$t\bar{t}$ Cross Section	0	10	0	0	0	0	0	0
Diboson Cross Section	0	0	6	6	0	0	0	0
$\sigma(p\bar{p} \to Z+HF)$	0	0	0	0	40	40	0	0
ISR/FSR	0	0	0	0	0	0	0	3
NN Trigger Model	0	5	5	5	5	5	0	5

Loose double tag (LDT) loose muons (missing E_T trigger) $ZH \to \ell\ell b\bar{b}$ channel relative uncertainties (%)

Contribution	Fakes	Top	WZ	ZZ	$Z+b\bar{b}$	$Z+c\bar{c}$	Z+mistag	ZH
Luminosity ($\sigma_{\rm inel}(p\bar{p})$)	0	3.8	3.8	3.8	3.8	3.8	0	3.8
Luminosity Monitor	0	4.4	4.4	4.4	4.4	4.4	0	4.4
Lepton ID	0	1	1	1	1	1	0	1
Lepton Energy Scale	0	1.5	1.5	1.5	1.5	1.5	0	1.5
ZH Cross Section	0	0	0	0	0	0	0	5
Fake Leptons	50	0	0	0	0	0	0	0
Jet Energy Scale (shape dep.)	0	$^{+0.0}_{-0.4}$	$^{+0.0}_{-0.0}$	$^{+0.0}_{-0.0}$	$^{+0.7}_{-0.3}$	$^{+0.0}_{-1.3}$	0	$^{+0.2}_{-0.2}$
Mistag Rate (shape dep.)	0	0	0	0	0	0	$^{+39.0}_{-29.5}$	0
B-Tag Efficiency	0	11	11	11	11	11	0	11
$t\bar{t}$ Cross Section	0	10	0	0	0	0	0	0
Diboson Cross Section	0	0	6	6	0	0	0	0
$\sigma(p\bar{p} \to Z+HF)$	0	0	0	0	40	40	0	0
ISR/FSR	0	0	0	0	0	0	0	1
NN Trigger Model	0	5	5	5	5	5	0	5

Tight double tag (TDT) loose muons (missing E_T trigger) $ZH \to \ell\ell b\bar{b}$ channel relative uncertainties (%)

Contribution	Fakes	Top	WZ	ZZ	$Z+b\bar{b}$	$Z+c\bar{c}$	Z+mistag	ZH
Luminosity ($\sigma_{\rm inel}(p\bar{p})$)	0	3.8	3.8	3.8	3.8	3.8	0	3.8
Luminosity Monitor	0	4.4	4.4	4.4	4.4	4.4	0	4.4
Lepton ID	0	1	1	1	1	1	0	1
Lepton Energy Scale	0	1.5	1.5	1.5	1.5	1.5	0	1.5
ZH Cross Section	0	0	0	0	0	0	0	5
Fake Leptons	50	0	0	0	0	0	0	0
Jet Energy Scale (shape dep.)	0	$^{+0.0}_{-0.0}$	$^{+0.0}_{-0.0}$	$^{+0.0}_{-0.0}$	$^{+0.4}_{-0.3}$	$^{+0.3}_{-0.1}$	0	$^{+0.5}_{-0.5}$
Mistag Rate (shape dep.)	0	0	0	0	0	0	$^{+29.7}_{-25.8}$	0
B-Tag Efficiency	0	8	8	8	8	8	0	8
$t\bar{t}$ Cross Section	0	10	0	0	0	0	0	0
Diboson Cross Section	0	0	6	6	0	0	0	0
$\sigma(p\bar{p} \to Z+HF)$	0	0	0	0	40	40	0	0
ISR/FSR	0	0	0	0	0	0	0	4
NN Trigger Model	0	5	5	5	5	5	0	5

TABLE XI: Observed and expected limits for all $ZH \to \ell^+\ell^- b\bar{b}$ channels combined. The observed and median expected limits are listed, as computed with the Markov chain method. Also listed are the limits from [27, 28]. The limits are all given in units of $R = \sigma/\sigma_{SM}$, assuming SM branching fractions..

m_H (GeV/c^2)	Observed limit/SM	median expected	CDF 10235,10221 observed	CDF 10235,10221 expected
100	4.36	5.23	4.35	5.15
105	4.67	5.03	4.64	5.07
110	5.16	5.02	5.13	5.19
115	6.05	5.43	5.99	5.48
120	7.55	6.62	7.51	6.42
125	9.06	8.15	8.96	8.16
130	12.20	11.20	12.09	11.20
135	16.16	15.53	16.05	16.37
140	24.06	25.16	23.79	26.21
145	34.22	41.71	33.40	42.62
150	61.12	72.86	59.81	73.72

TABLE XII: Systematic uncertainties on the signal and background contributions for the $H \to \tau^+\tau^-$ channels. Systematic uncertainties are listed by name; see the original references for a detailed explanation of their meaning and on how they are derived. Systematic uncertainties for the Higgs signal shown in these tables are obtained for $m_H = 120$ GeV/c^2. Uncertainties are relative, in percent, and are symmetric unless otherwise indicated.

$H \to \tau^+\tau^-$ channel relative uncertainties (%)

Contribution	$Z/\gamma^* \to ll$	$t\bar{t}$	diboson	fakes from SS	W+jets	WH	ZH	VBF	$gg \to H$
PDF Uncertainty	1	1	1	-	-	1.2	0.9	2.2	4.9
ISR 1 JET	-	-	-	-	-	-6.1	-1.7	-2.9	13.0
ISR $\geq$ 2 JETS	-	-	-	-	-	-1.5	0.1	-2.7	15.5
FSR 1 JET	-	-	-	-	-	4.3	1.0	1.7	-5.0
FSR $\geq$ 2 JETS	-	-	-	-	-	-2.1	0.4	-1.1	-5.2
JES (shape) 1 JET	6.2	-7.7	7.1	-	-	-4.8	-5.3	-3.7	5.1
JES (shape) $\geq$ 2 JETS	14.2	3.2	11.7	-	-	5.4	4.8	-5.2	13.2
Cross Section or Norm. 1 JET	2.2	10	6	10	18	5	5	10	23.5
Cross Section or Norm. $\geq$2 JETS	2.2	10	6	10	30	5	5	10	67.5
MC Acceptance	2.3	-	-	-	-	-	-	-	-
tau ID scale factor:									
N_{obs}	2.8	2.8	2.8	-	-	2.8	2.8	2.8	2.8
N_{SSdata}	-3.3	-3.3	-3.3	-	-	-3.3	-3.3	-3.3	-3.3
N_{W+jets}	-0.3	-0.3	-0.3	-	-	-0.3	-0.3	-0.3	-0.3
Cross section (DY)	-2.1	-2.1	-2.1	-	-	-2.1	-2.1	-2.1	-2.1
MC Acceptance (DY)	-2.2	-2.2	-2.2	-	-	-2.2	-2.2	-2.2	-2.2

TABLE XIII: Observed and expected limits for the $H \to \tau^+\tau^-$ channel. The observed and median expected limits calculated with the Markov chain method are listed. Also listed are the limits from [41]. The limits are all given in units of $R = \sigma/\sigma_{SM}$, assuming SM branching fractions.

m_H (GeV/c^2)	Observed limit/SM	median expected	CDF 10113 observed	CDF 10113 expected
100	35.53	28.44	37.6	28.2
105	32.78	25.39	34.5	25.2
110	33.08	24.44	34.8	23.9
115	26.77	24.28	27.9	24.5
120	25.95	23.31	27.2	23.4
125	24.03	25.98	25.3	26.5
130	28.56	28.29	30.0	28.1
135	28.61	32.32	30.3	33.7
140	36.06	41.44	38.2	41.2
145	43.85	56.20	46.3	57.4
150	63.37	81.78	67.0	82.6

TABLE XIV: Systematic uncertainties on the signal and background contributions for the $WH+ZH \to jjbb$ and $VBF \to jjbb$ channels. Systematic uncertainties are listed by name; see the original references for a detailed explanation of their meaning and on how they are derived. Uncertainties with provided shape systematics are labeled with "s". Systematic uncertainties for H shown in this table are obtained for $m_H = 115$ GeV/c^2. Uncertainties are relative, in percent, and are symmetric unless otherwise indicated. The cross section uncertainties are uncorrelated with each other (except for single top and $t\bar{t}$, which are treated as correlated). The QCD uncertainty is also uncorrelated with other channels' QCD rate uncertainties.

$WH + ZH \to jjbb$ and $VBF \to jjbb$ channel relative uncertainties (%)

Contribution	$t\bar{t}$	diboson	W/Z+Jets	VH	VBF
Jet Energy Correction				7 s	7 s
PDF Modeling				2	2
SecVtx+SecVtx	7.6	7.6	7.6	7.6	7.6
SecVtx+JetProb	9.7	9.7	9.7	9.7	9.7
Luminosity	6	6	6	6	6
ISR/FSR modeling				2 s	3 s
Jet Moment				s	s
Trigger	4	4	4	4	4
QCD Interpolation				s	s
QCD MJJ Tuning				s	s
QCD Jet Moment Tuning				s	s
cross section	10	6	50		

TABLE XV: Observed and expected limits for the $WH + ZH \to jjb\bar{b}$ channel. The observed and median expected limits calculated with the Markov chain method are listed. Also listed are the limits from [42]. The limits are all given in units of $R = \sigma/\sigma_{SM}$, assuming SM branching fractions.

m_H (GeV/c^2)	Observed limit/SM	median expected	CDF 10010 observed	CDF 10010 expected
100	10.61	19.83	10.1	18.8
105	10.69	18.12	9.9	17.4
110	10.53	17.61	10.2	17.1
115	10.40	18.68	9.1	17.8
120	11.45	20.74	10.5	20.0
125	15.04	29.22	13.8	27.3
130	18.92	38.47	17.2	36.1
135	24.90	43.02	22.7	41.9
140	36.67	64.87	35.2	60.4
145	61.87	104.39	55.8	95.7
150	110.57	176.02	101.0	164.1

TABLE XVI: Systematic uncertainties on the signal and background contributions for the $H \to W^+W^- \to \ell^\pm\ell'^\mp$ channels with zero, one, and two or more associated jets. These channels are sensitive to gluon fusion production (all channels) and WH, ZH and VBF production. Systematic uncertainties are listed by name (see the original references for a detailed explanation of their meaning and on how they are derived). Systematic uncertainties for H shown in this table are obtained for $m_H = 160$ GeV/c^2. Uncertainties are relative, in percent, and are symmetric unless otherwise indicated. The uncertainties associated with the different background and signal processed are correlated within individual jet categories unless otherwise noted. Boldface and italics indicate groups of uncertainties which are correlated with each other but not the others on the line.

$H \to W^+W^- \to \ell^\pm\ell'^\mp$ with no associated jet channel relative uncertainties (%)

Contribution	WW	WZ	ZZ	$t\bar{t}$	DY	$W\gamma$	W+jet	$gg \to H$	WH	ZH	VBF
Cross Section :											
Scale								7.0			
PDF Model								7.6			
Total	*6.0*	*6.0*	*6.0*	10.0					**5.0**	**5.0**	10.0
Acceptance :											
Scale (leptons)								1.7			
Scale (jets)	*0.3*							1.5			
PDF Model (leptons)								2.7			
PDF Model (jets)	*1.1*							5.5			
Higher-order Diagrams		*10.0*	*10.0*	10.0		10.0			**10.0**	**10.0**	**10.0**
$\not\!\!E_T$ Modeling					19.5						
Conversion Modeling						10.0					
Jet Fake Rates											
(Low S/B)							22.0				
(High S/B)							25.0				
Jet Energy Scale	*2.6*	*6.1*	*3.4*	*26.0*	*17.5*	*3.1*		*5.0*	*10.5*	*5.0*	*11.5*
Lepton ID Efficiencies	*3.0*	*3.0*	*3.0*	*3.0*	*3.0*			*3.0*	*3.0*	*3.0*	*3.0*
Trigger Efficiencies	*2.0*	*2.0*	*2.0*	*2.0*	*2.0*			*2.0*	*2.0*	*2.0*	*2.0*
Luminosity	*3.8*	*3.8*	*3.8*	*3.8*	*3.8*			*3.8*	*3.8*	*3.8*	*3.8*
Luminosity Monitor	*4.4*	*4.4*	*4.4*	*4.4*	*4.4*			*4.4*	*4.4*	*4.4*	*4.4*

$H \to W^+W^- \to \ell^\pm\ell'^\mp$ with one associated jet channel relative uncertainties (%)

Contribution	WW	WZ	ZZ	$t\bar{t}$	DY	$W\gamma$	W+jet	$gg \to H$	WH	ZH	VBF
Cross Section :											
Scale								23.5			
PDF Model								17.3			
Total	*6.0*	*6.0*	*6.0*	10.0					**5.0**	**5.0**	10.0
Acceptance :											
Scale (leptons)								2.2			
Scale (jets)	*-4.0*							-1.9			
PDF Model (leptons)								*3.6*			
PDF Model (jets)	*4.7*							-6.3			
Higher-order Diagrams		*10.0*	*10.0*	10.0		10.0			**10.0**	**10.0**	**10.0**
$\not\!\!E_T$ Modeling					20.0						
Conversion Modeling						10.0					
Jet Fake Rates											
(Low S/B)							23.0				
(High S/B)							28.0				
Jet Energy Scale	*-5.5*	*-1.0*	*-4.3*	*-13.0*	*-6.5*	*-9.5*		*-4.0*	*-8.5*	*-7.0*	*-6.5*
Lepton ID Efficiencies	*3.0*	*3.0*	*3.0*	*3.0*	*3.0*			*3.0*	*3.0*	*3.0*	*3.0*
Trigger Efficiencies	*2.0*	*2.0*	*2.0*	*2.0*	*2.0*			*2.0*	*2.0*	*2.0*	*2.0*
Luminosity	*3.8*	*3.8*	*3.8*	*3.8*	*3.8*			*3.8*	*3.8*	*3.8*	*3.8*
Luminosity Monitor	*4.4*	*4.4*	*4.4*	*4.4*	*4.4*			*4.4*	*4.4*	*4.4*	*4.4*

$H \to W^+W^- \to \ell^\pm\ell'^\mp$ with two or more associated jets channel relative uncertainties (%)

Contribution	WW	WZ	ZZ	$t\bar{t}$	DY	$W\gamma$	W+jet	$gg \to H$	WH	ZH	VBF
Cross Section :											
Scale								67.5			
PDF Model								29.7			
Total	*6.0*	*6.0*	*6.0*	10.0					**5.0**	**5.0**	10.0
Acceptance :											
Scale (leptons)								3.1			
Scale (jets)	*-8.2*							-6.8			
PDF Model (leptons)								*4.8*			
PDF Model (jets)	*4.2*							-12.3			
Higher-order Diagrams		*10.0*	*10.0*	10.0		10.0			**10.0**	**10.0**	**10.0**
$\not{E}_T$ Modeling					25.5						
Conversion Modeling						10.0					
Jet Fake Rates							28.0				
Jet Energy Scale	*-14.8*	*-12.9*	*-12.1*	*-1.7*	*-29.2*	*-22.0*		*-17.0*	*-4.0*	*-2.3*	*-4.0*
b-tag Veto				3.8							
Lepton ID Efficiencies	*3.0*	*3.0*	*3.0*	*3.0*	*3.0*			*3.0*	*3.0*	*3.0*	*3.0*
Trigger Efficiencies	*2.0*	*2.0*	*2.0*	*2.0*	*2.0*			*2.0*	*2.0*	*2.0*	*2.0*
Luminosity	*3.8*	*3.8*	*3.8*	*3.8*	*3.8*			*3.8*	*3.8*	*3.8*	*3.8*
Luminosity Monitor	*4.4*	*4.4*	*4.4*	*4.4*	*4.4*			*4.4*	*4.4*	*4.4*	*4.4*

TABLE XVII: Systematic uncertainties on the signal and background contributions for the low-$M_{\ell\ell}$ $H \to W^+W^- \to \ell^\pm\ell'^\mp$ channel with zero or one associated jets. This channel is sensitive to only gluon fusion production. Systematic uncertainties are listed by name (see the original references for a detailed explanation of their meaning and on how they are derived). Systematic uncertainties for H shown in this table are obtained for $m_H = 160$ GeV/c^2. Uncertainties are relative, in percent, and are symmetric unless otherwise indicated. The uncertainties associated with the different background and signal processed are correlated within individual categories unless otherwise noted. In these special cases, the correlated uncertainties are shown in either italics or bold face text.

Low $M_{\ell\ell}$ $H \to W^+W^- \to \ell^\pm\ell'^\mp$ with zero or one associated jets channel relative uncertainties (%)

Contribution	WW	WZ	ZZ	$t\bar{t}$	DY	$W\gamma$	W+jet(s)	$gg \to H$
Cross Section :								
Scale								12.0
PDF Model								10.7
Total	*6.0*	*6.0*	*6.0*	10.0	5.0			16.1
Acceptance :								
Scale (leptons)								0.6
Scale (jets)								1.2
PDF Model (leptons)								*1.0*
PDF Model (jets)	*1.6*							2.1
Higher-order Diagrams		10.0	10.0	10.0	10.0			
Jet Energy Scale	*1.0*	*2.3*	*2.0*	*12.9*	*6.4*	*1.3*		*2.4*
Conversion Modeling						10.0		
Jet Fake Rates							18.4	
Lepton ID Efficiencies	*3.0*	*3.0*	*3.0*	*3.0*	*3.0*			*3.0*
Trigger Efficiencies	*2.0*	*2.0*	*2.0*	*2.0*	*2.0*			*2.0*
Luminosity	*3.8*	*3.8*	*3.8*	*3.8*	*3.8*			*3.8*
Luminosity Monitor	*4.4*	*4.4*	*4.4*	*4.4*	*4.4*			*4.4*

TABLE XVIII: Systematic uncertainties on the signal and background contributions for the $H \to W^+W^- \to e^\pm\tau^\mp$ and $H \to W^+W^- \to \mu^\pm\tau^\mp$ channels. These channels are sensitive to gluon fusion production, WH, ZH and VBF production. Systematic uncertainties are listed by name (see the original references for a detailed explanation of their meaning and on how they are derived). Systematic uncertainties for H shown in this table are obtained for $m_H = 160$ GeV/c^2. Uncertainties are relative, in percent, and are symmetric unless otherwise indicated. The uncertainties associated with the different background and signal processed are correlated within individual categories unless otherwise noted. In these special cases, the correlated uncertainties are shown in either italics or bold face text.

$H \to W^+W^- \to e^\pm\tau^\mp$ channel relative uncertainties (%)

Contribution	WW	WZ	ZZ	$t\bar{t}$	$Z \to \tau\tau$	$Z \to \ell\ell$	W+jet	$W\gamma$	$gg \to H$	WH	ZH	VBF
Cross section	6.0	6.0	6.0	10.0	5.0	5.0			10.3	5	5	10
Measured W cross-section							12					
PDF Model	1.6	2.3	3.2	2.3	2.7	4.6	2.2	3.1	2.5	2.0	1.9	1.8
Higher order diagrams	10	10	10	10	10	10		10		10	10	10
Conversion modeling								10				
Trigger Efficiency	0.5	0.6	0.6	0.6	0.7	0.5	0.6	0.6	0.5	0.5	0.6	0.5
Lepton ID Efficiency	0.4	0.5	0.5	0.4	0.4	0.4	0.5	0.4	0.4	0.4	0.4	0.4
τ ID Efficiency	1.0	1.3	1.9	1.3	2.1			0.3	2.8	1.6	1.7	2.8
Jet into τ Fake rate	5.8	4.8	2.0	5.1		0.1	8.8			4.2	4.0	0.4
Lepton into τ Fake rate	0.2	0.1	0.6	0.2		2.3		2.1	0.15	0.06	0.15	0.11
W+jet scale							1.6					
MC Run dependence	2.6	2.6	2.6				2.6					
Luminosity	3.8	3.8	3.8	3.8	3.8	3.8	3.8	3.8	3.8	3.8	3.8	3.8
Luminosity Monitor	4.4	4.4	4.4	4.4	4.4	4.4	4.4	4.4	4.4	4.4	4.4	4.4

$H \to W^+W^- \to \mu^\pm\tau^\mp$ channel relative uncertainties (%)

Contribution	WW	WZ	ZZ	$t\bar{t}$	$Z \to \tau\tau$	$Z \to \ell\ell$	W+jet	$W\gamma$	$gg \to H$	WH	ZH	VBF
Cross section	6.0	6.0	6.0	10.0	5.0	5.0			10.4	5	5	10
Measured W cross-section							12					
PDF Model	1.5	2.1	2.9	2.1	2.5	4.3	2.0	2.9	2.6	2.2	2.0	2.2
Higher order diagrams	10	10	10	10				11		10	10	10
Trigger Efficiency	1.3	0.7	0.7	1.1	0.9	1.3	1.0	1.0	1.3	1.3	1.2	1.3
Lepton ID Efficiency	1.1	1.4	1.4	1.1	1.2	1.1	1.4	1.3	1.0	1.0	1.0	1.0
τ ID Efficiency	1.0	1.2	1.4	1.6	1.9				2.9	1.6	1.7	2.8
Jet into τ Fake rate	5.8	5.0	4.4	4.4		0.2	8.8			4.5	4.2	0.4
Lepton into τ Fake rate	0.06	0.05	0.09	0.04		1.9		1.2	0.04	0.02	0.02	0.04
W+jet scale							1.4					
MC Run dependence	3.0	3.0	3.0				3.0					
Luminosity	3.8	3.8	3.8	3.8	3.8	3.8	3.8	3.8	3.8	3.8	3.8	3.8
Luminosity Monitor	4.4	4.4	4.4	4.4	4.4	4.4	4.4	4.4	4.4	4.4	4.4	4.4

TABLE XIX: Systematic uncertainties on the signal and background contributions for the $WH \to WWW \to \ell^{\pm}\ell'^{\pm}$ channel with one or more associated jets and $WH \to WWW \to \ell^{\pm}\ell'^{\pm}\ell''^{\mp}$ channel. These channels are sensitive to only WH and ZH production. Systematic uncertainties are listed by name (see the original references for a detailed explanation of their meaning and on how they are derived). Systematic uncertainties for H shown in this table are obtained for $m_H = 160$ GeV/c^2. Uncertainties are relative, in percent, and are symmetric unless otherwise indicated. The uncertainties associated with the different background and signal processed are correlated within individual categories unless otherwise noted. In these special cases, the correlated uncertainties are shown in either italics or bold face text.

$WH \to WWW \to \ell^{\pm}\ell'^{\pm}$ channel relative uncertainties (%)

Contribution	WW	WZ	ZZ	$t\bar{t}$	DY	$W\gamma$	W+jet	WH	ZH
Cross Section	*6.0*	*6.0*	*6.0*	10.0	5.0			**5.0**	**5.0**
Scale (Acceptance)	*-6.1*								
PDF Model (Acceptance)	*5.7*								
Higher-order Diagrams		*10.0*	*10.0*	10.0	10.0	10.0		**10.0**	**10.0**
Conversion Modeling						10.0			
Jet Fake Rates							39.1		
Jet Energy Scale	*-14.0*	*-3.9*	*-2.8*	*-0.6*	*-9.3*	*-7.6*		*-1.0*	*-0.7*
Charge Mismeasurement Rate	*19.0*			*19.0*	*19.0*				
Lepton ID Efficiencies	*3.0*	*3.0*	*3.0*	*3.0*	*3.0*			*3.0*	*3.0*
Trigger Efficiencies	*2.0*	*2.0*	*2.0*	*2.0*	*2.0*			*2.0*	*2.0*
Luminosity	*3.8*	*3.8*	*3.8*	*3.8*	*3.8*			*3.8*	*3.8*
Luminosity Monitor	*4.4*	*4.4*	*4.4*	*4.4*	*4.4*			*4.4*	*4.4*

$WH \to WWW \to \ell^{\pm}\ell'^{\pm}\ell''^{\mp}$ channel relative uncertainties (%)

Contribution	WZ	ZZ	$Z\gamma$	$t\bar{t}$	Fakes	WH	ZH
Cross Section	*6.0*	*6.0*	10.0	10.0		**5.0**	**5.0**
Higher-order Diagrams	*10.0*	*10.0*	15.0	10.0		**10.0**	**10.0**
Jet Energy Scale			*-2.7*				
Jet Fake Rates					24.8		
b-Jet Fake Rates				27.3			
MC Run Dependence			5.0				
Lepton ID Efficiencies	*3.0*	*3.0*		*3.0*		*3.0*	*3.0*
Trigger Efficiencies	*2.0*	*2.0*		*2.0*		*2.0*	*2.0*
Luminosity	*3.8*	*3.8*		*3.8*		*3.8*	*3.8*
Luminosity Monitor	*4.4*	*4.4*		*4.4*		*4.4*	*4.4*

TABLE XX: Systematic uncertainties on the signal and background contributions for the $ZH \to ZWW \to \ell^{\pm}\ell^{\mp}\ell'^{\pm}$ channels with 1 jet and 2 or more jets. These channels are sensitive to only WH and ZH production. Systematic uncertainties are listed by name (see the original references for a detailed explanation of their meaning and on how they are derived). Systematic uncertainties for H shown in this table are obtained for $m_H = 160$ GeV/c^2. Uncertainties are relative, in percent, and are symmetric unless otherwise indicated. The uncertainties associated with the different background and signal processed are correlated within individual categories unless otherwise noted. In these special cases, the correlated uncertainties are shown in either italics or bold face text.

$ZH \to ZWW \to \ell^{\pm}\ell^{\mp}\ell'^{\pm}$ with one associated jet channel relative uncertainties (%)

Contribution	WZ	ZZ	$Z\gamma$	$t\bar{t}$	Fakes	WH	ZH
Cross Section	*6.0*	*6.0*	10.0	10.0		**5.0**	**5.0**
Higher-order Diagrams	*10.0*	*10.0*	15.0	10.0		**10.0**	**10.0**
Jet Energy Scale	*-7.6*	*-2.3*	*-5.3*	*9.4*		*-9.0*	*8.1*
Jet Fake Rates					25.8		
b-Jet Fake Rates				42.0			
MC Run Dependence			5.0				
Lepton ID Efficiencies	*3.0*	*3.0*		*3.0*		*3.0*	*3.0*
Trigger Efficiencies	*2.0*	*2.0*		*2.0*		*2.0*	*2.0*
Luminosity	*3.8*	*3.8*		*3.8*		*3.8*	*3.8*
Luminosity Monitor	*4.4*	*4.4*		*4.4*		*4.4*	*4.4%*

$ZH \to ZWW \to \ell^{\pm}\ell^{\mp}\ell'^{\pm}$ with two or more associated jets channel relative uncertainties (%)

Contribution	WZ	ZZ	$Z\gamma$	$t\bar{t}$	Fakes	WH	ZH
Cross Section	*6.0*	*6.0*	10.0	10.0		**5.0**	**5.0**
Higher-order Diagrams	*10.0*	*10.0*	15.0	10.0		**10.0**	**10.0**
Jet Energy Scale	*-17.8*	*-13.1*	*-18.2*	*-3.6*		*-15.4*	*-4.9*
Jet Fake Rates					25.4		
b-Jet Fake Rates				22.2			
MC Run Dependence			5.0				
Lepton ID Efficiencies	*3.0*	*3.0*		*3.0*		*3.0*	*3.0*
Trigger Efficiencies	*2.0*	*2.0*		*2.0*		*2.0*	*2.0*
Luminosity	*3.8*	*3.8*		*3.8*		*3.8*	*3.8*
Luminosity Monitor	*4.4*	*4.4*		*4.4*		*4.4*	*4.4*

TABLE XXI: Observed and expected limits for the $gg \to H \to W^+W^- \to$ leptons+$\not\!\!E_T$ channels in combination, including the five opposite-sign channels, the low-$m_{\ell\ell}$ channel, the same-sign channel, the three trilepton channels, and the two channels including the hadronic tau final states. The observed and median expected limits computed with the Markov chain technique are listed. Also listed are the limits from [43]. The limits are all given in units of $R = \sigma/\sigma_{SM}$, assuming SM branching fractions.

m_H (GeV/c^2)	Observed limit/SM	median expected	CDF 10232 observed	CDF 10232 expected
110	23.28	19.62	22.98	19.90
115	13.40	10.51	13.12	10.59
120	6.91	6.71	6.65	6.74
125	5.58	4.51	5.37	4.50
130	4.28	3.46	4.10	3.42
135	3.26	2.69	3.13	2.74
140	2.84	2.24	2.68	2.28
145	2.36	1.94	2.23	1.95
150	2.62	1.67	2.51	1.67
155	1.79	1.43	1.74	1.40
160	1.37	1.05	1.32	1.05
165	1.13	1.00	1.08	1.00
170	1.32	1.20	1.28	1.20
175	1.59	1.36	1.54	1.42
180	2.34	1.70	2.24	1.70
185	3.66	2.18	3.57	2.17
190	3.37	2.66	3.23	2.67
195	4.92	3.17	4.79	3.23
200	5.47	3.56	5.24	3.57

TABLE XXII: Systematic uncertainties on the signal and background contributions for the $H \to \gamma\gamma$ channel. Systematic uncertainties for the Higgs signal shown in this table are obtained for $m_H = 120$ GeV/c^2. Systematic uncertainties are listed by name; see the original references for a detailed explanation of their meaning and on how they are derived. Uncertainties are relative, in percent, and are symmetric unless otherwise indicated.

$H \to \gamma\gamma$ channel relative uncertainties (%)

Contribution	background	signal
Luminosity		6
σ_{ggH} / σ_{VH} / σ_{VBF}		12 / 5 / 10
PDF		1
ISR		2
FSR		2
Energy Scale		0.1
Vertex		0.2
Conversions		0.2
Photon/Electron ID		1.0
Run Dependence		1.5
Data/MC fits		0.2
Background Shape	4	

TABLE XXIII: Observed and expected limits for the $H \to \gamma\gamma$ channel. The observed and median expected limits computed with the Markov chain technique are listed, along with the limits from [29]. The limits are all given in units of $R = \sigma/\sigma_{SM}$, assuming SM branching fractions.

m_H (GeV/c^2)	Observed limit/SM	median expected	CDF 10065 observed	CDF 10065 expected
100	24.20	25.83	24.3	25.7
105	18.19	23.18		
110	26.38	21.50	25.9	21.5
115	24.13	20.26		
120	23.19	19.94	22.5	19.4
125	21.74	20.09		
130	18.97	21.13	18.7	20.6
135	21.61	23.26		
140	33.13	25.64	32.9	25.5
145	36.48	30.95		
150	41.30	39.80	40.0	38.6

TABLE XXIV: Observed and expected limits for all CDF SM Higgs boson search channels combined, usng the Markov chain method. The observed and median expected limits are listed, as well as $\pm 1, 2\sigma$ variation on the expected limits from statistical fluctuations assuming only background processes contribute. The limits are all given in units of $R = \sigma/\sigma_{SM}$, assuming SM branching fractions.

m_H (GeV/c^2)	Observed limit/SM	-2σ expected	-1σ expected	median expected	$+1\sigma$ expected	$+2\sigma$ expected
100	0.86	0.83	1.11	1.55	2.18	3.02
105	1.07	0.90	1.18	1.63	2.28	3.17
110	1.59	0.96	1.30	1.81	2.53	3.50
115	1.79	1.00	1.37	1.90	2.61	3.52
120	2.13	1.10	1.59	2.26	3.12	4.22
125	2.28	1.23	1.66	2.28	3.11	4.18
130	2.56	1.25	1.68	2.33	3.23	4.44
135	2.23	1.22	1.65	2.28	3.15	4.30
140	2.24	1.08	1.47	2.04	2.84	3.90
145	2.16	1.01	1.31	1.84	2.65	3.80
150	2.40	0.84	1.14	1.60	2.24	3.10
155	1.79	0.74	1.01	1.43	2.05	2.90
160	1.37	0.55	0.75	1.05	1.49	2.08
165	1.13	0.54	0.72	1.00	1.41	1.96
170	1.32	0.63	0.84	1.20	1.72	2.45
175	1.59	0.76	0.98	1.36	1.92	2.69
180	2.34	0.91	1.21	1.70	2.42	3.41
185	3.66	1.16	1.56	2.18	3.07	4.27
190	3.37	1.49	1.93	2.66	3.75	5.25
195	4.92	1.77	2.30	3.17	4.46	6.24
200	5.47	1.87	2.53	3.56	5.04	7.06

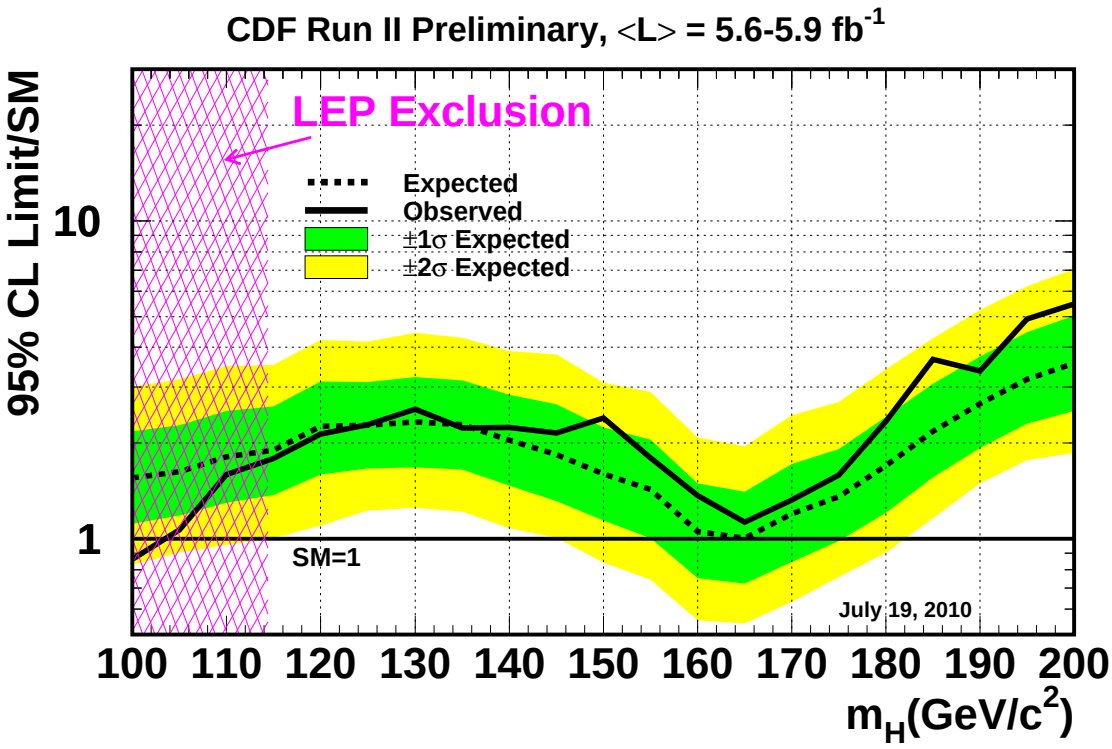

FIG. 1: The 95% CL upper limit on $R = \sigma/\sigma_{\rm SM}$, shown as a function of m_H, for the combination of all of CDF's SM Higgs search channels. The $\pm 1, 2\sigma$ bands on the expected limits are also shown, centered on the median expected limit.

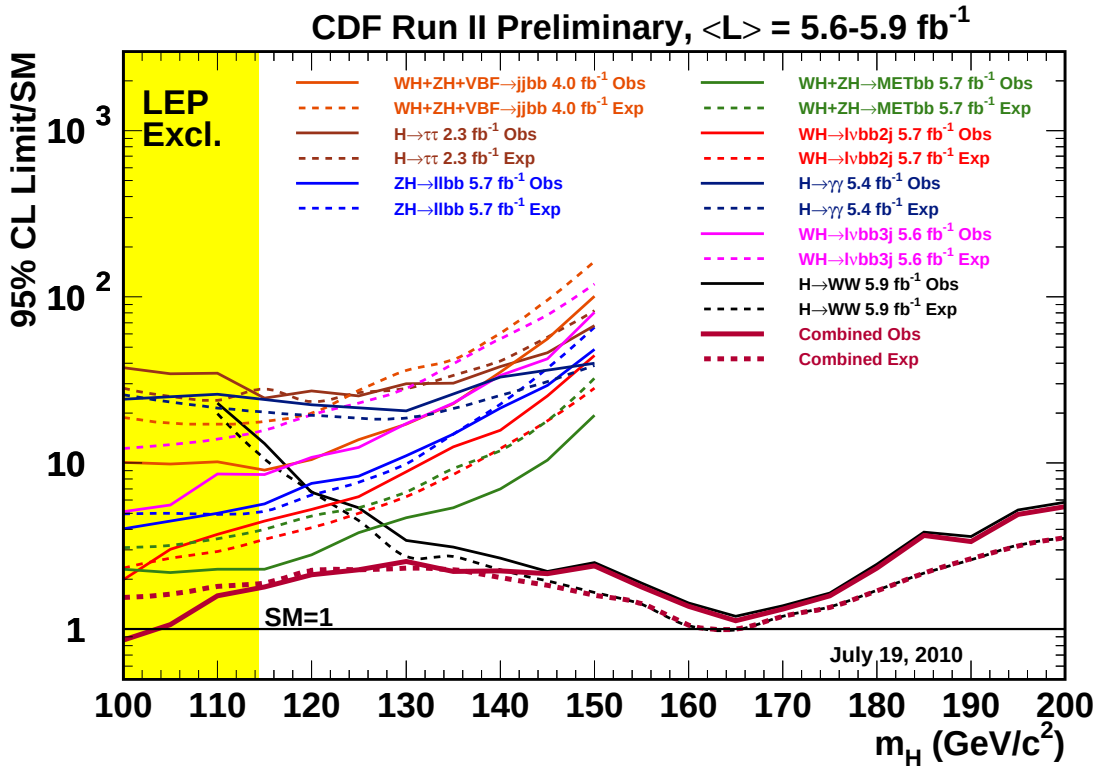

FIG. 2: The 95% CL upper limit on $R = \sigma/\sigma_{\rm SM}$, shown as a function of m_H, shown separately for each analysis and for the combination. Dashed lines indicate the median expected limits, and the solid lines show the observed limits. The individual analysis limits are those approved by the individual analyses, and the combined limit is documented in this note. The $WH \to \ell\nu b\bar{b}$ limits are the combination of the 2J and 3J channels. The LEP bound $m_H > 114.4$ GeV/c^2 is shown in yellow.

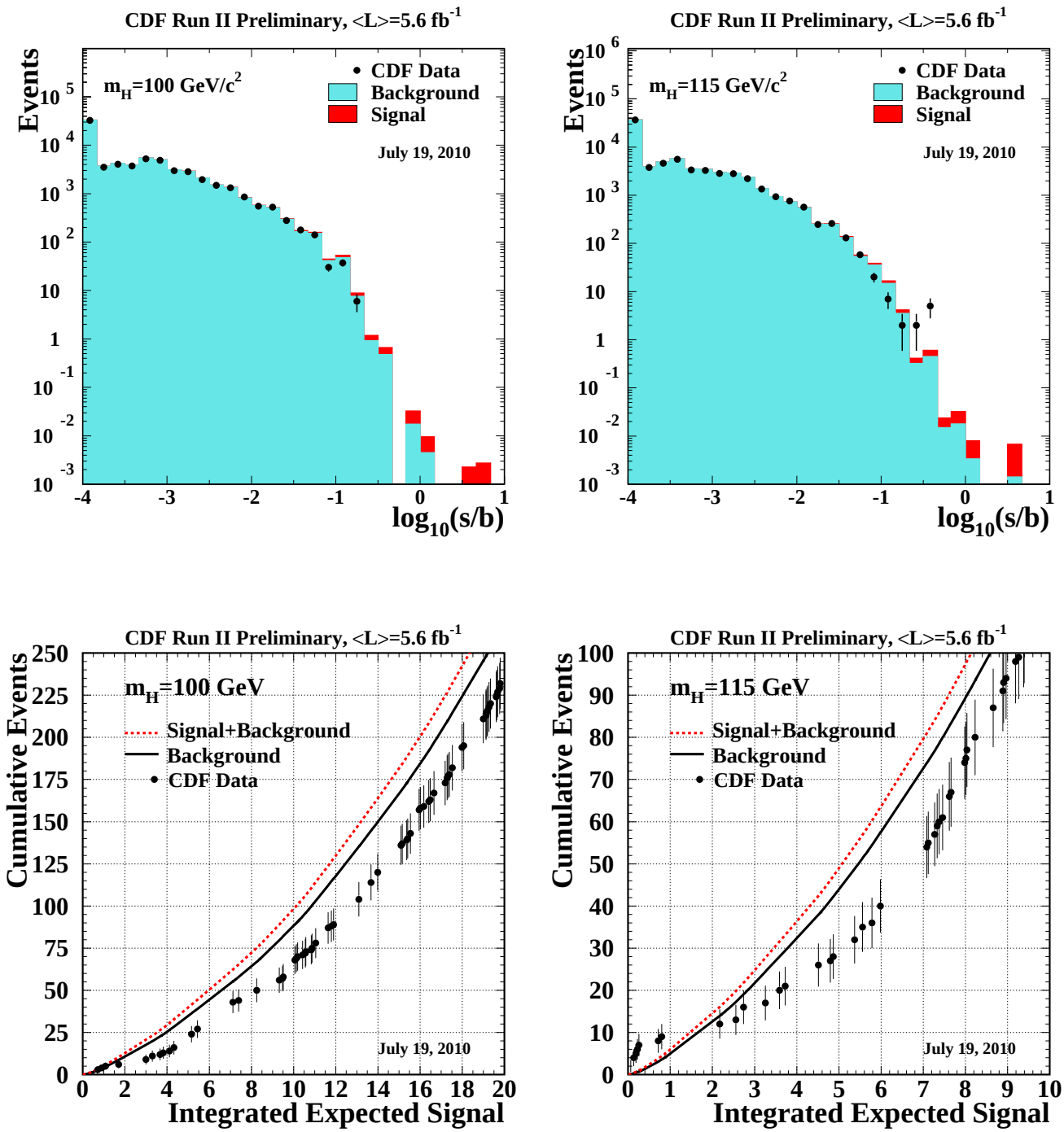

FIG. 3: Top plots: signal predictions, background predictions, and observed data, collected in bins sorted by s/b, for all channels added together. These are shown for m_H=100 and 115 GeV/c^2. Bottom plots: Integrated signal predictions, background predictions, and observed data, collected in bins sorted by s/b, for all channels added together. These are shown for m_H=100 and 115 GeV/c^2.

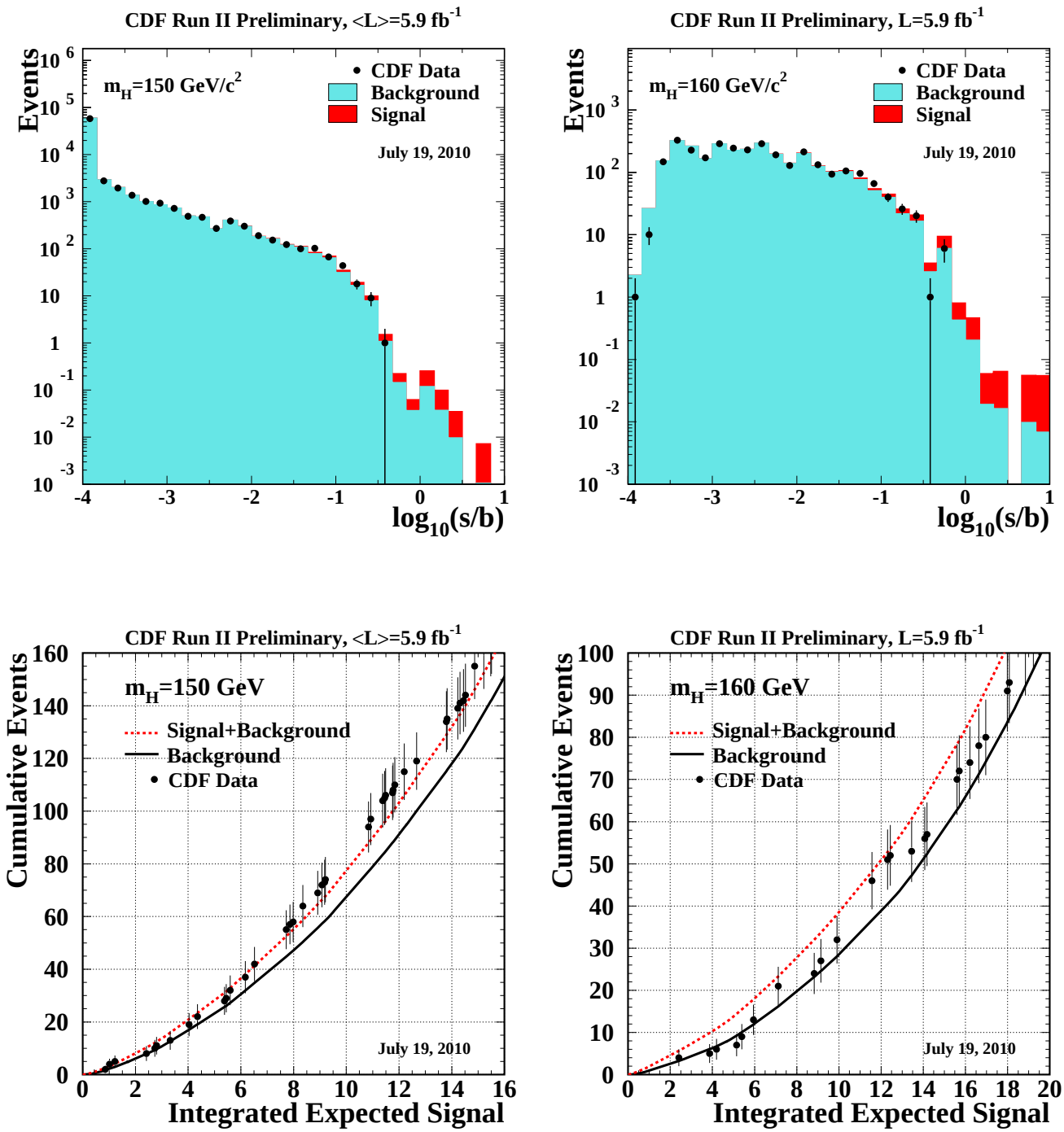

FIG. 4: Top plots: signal predictions, background predictions, and observed data, collected in bins sorted by s/b, for all channels added together. These are shown for m_H=150 and 160 GeV/c^2. Bottom plots: Integrated signal predictions, background predictions, and observed data, collected in bins sorted by s/b, for all channels added together. These are shown for m_H=150 and 160 GeV/c^2.

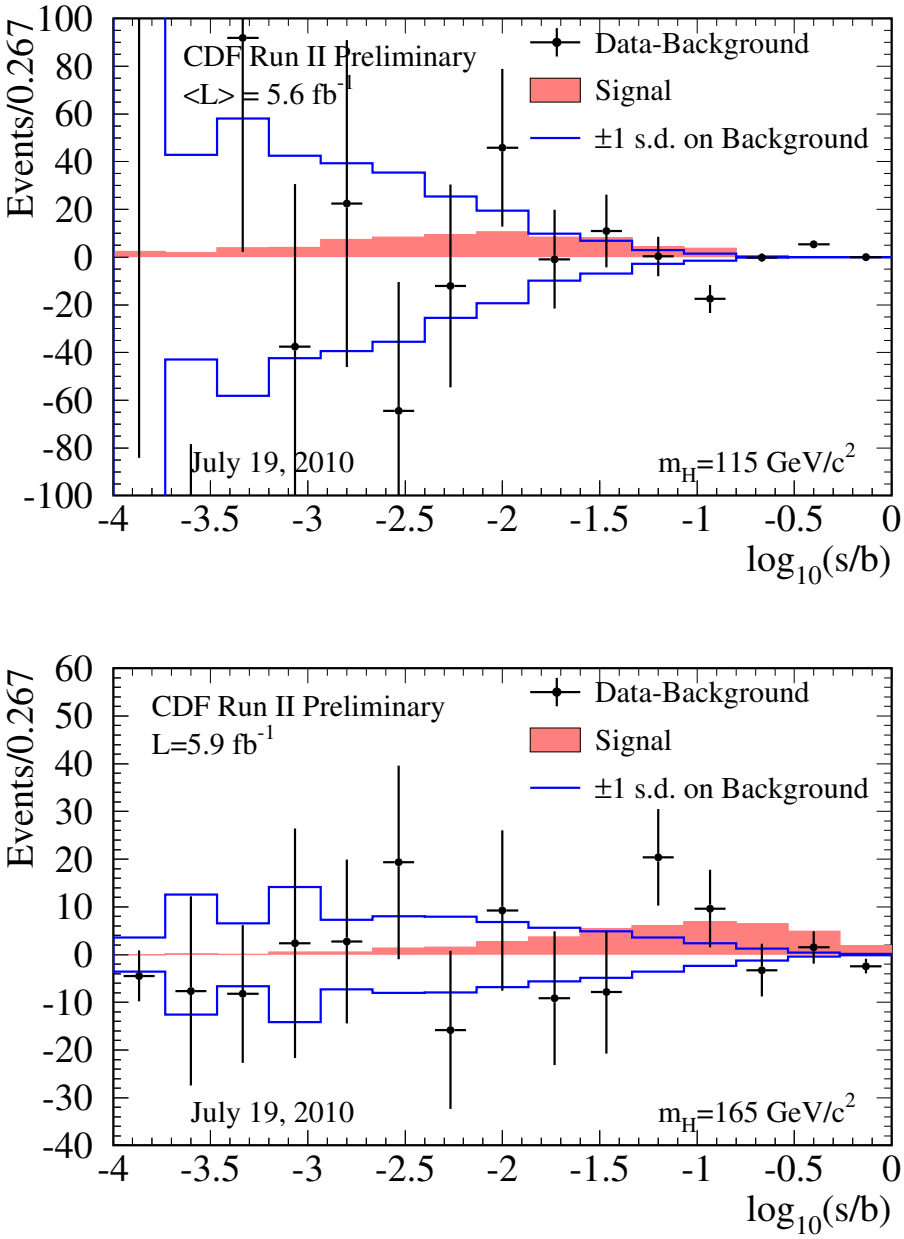

FIG. 5: Background-subtracted data distributions for the $m_H = 115$ GeV/c^2 search (top plot) and the $m_H = 165$ GeV/c^2 search (bottom plot), sorted by s/b and summed over all channels. The background has been fit to the data, and the empty histograms show the residual uncertainty on the background after the fit. The shaded histograms show the signal prediction, and the points with error bars show the data after the fit background. The error bars are the square roots of the background rates in their bins, after the fit.

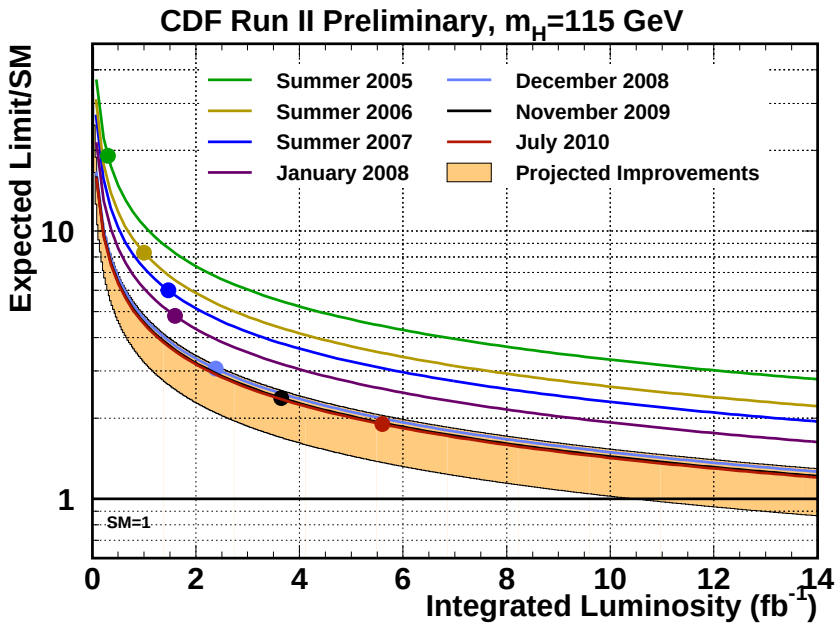

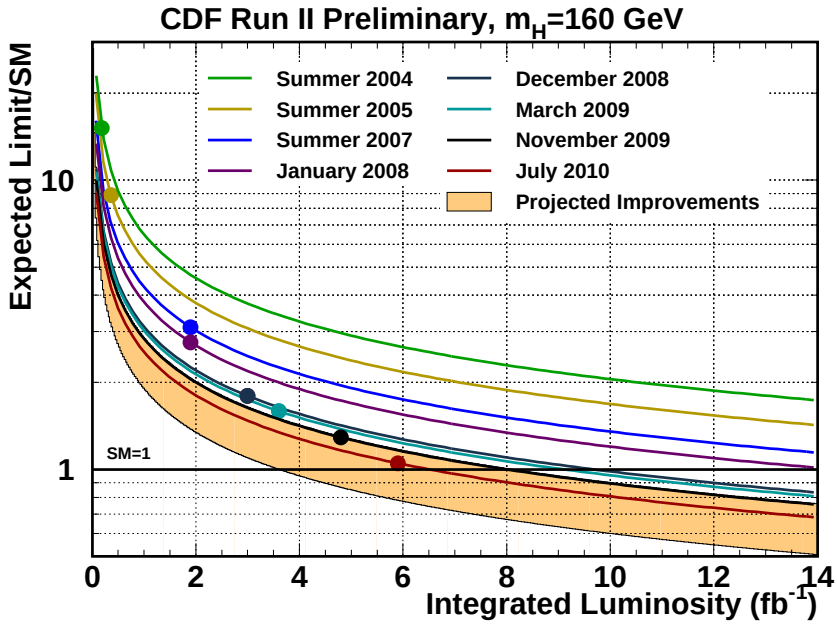

FIG. 6: Sensitivity projections and achieved sensitivities for the combined CDF Higgs boson searches, at $m_H = 115$ and 160 GeV/c^2. The curves are proportional to $1/\sqrt{\int Ldt}$ extrapolations of the median expected limits, and each analysis update corresponds to a new point with a new curve. The light orange bands indicate ranges of possible improvements in performance, relative to the Summer 2007 sensitivity. The top of the light orange bands is a factor of 1.5 below the Summer 2007 curve, and the bottom of the light orange bands are a further factor of 1.5 below the top of the light orange bands.

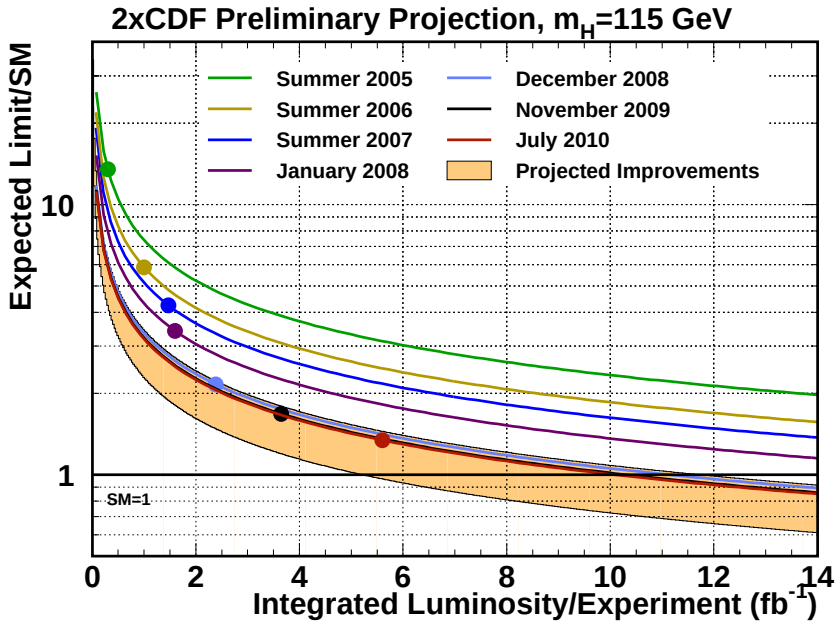

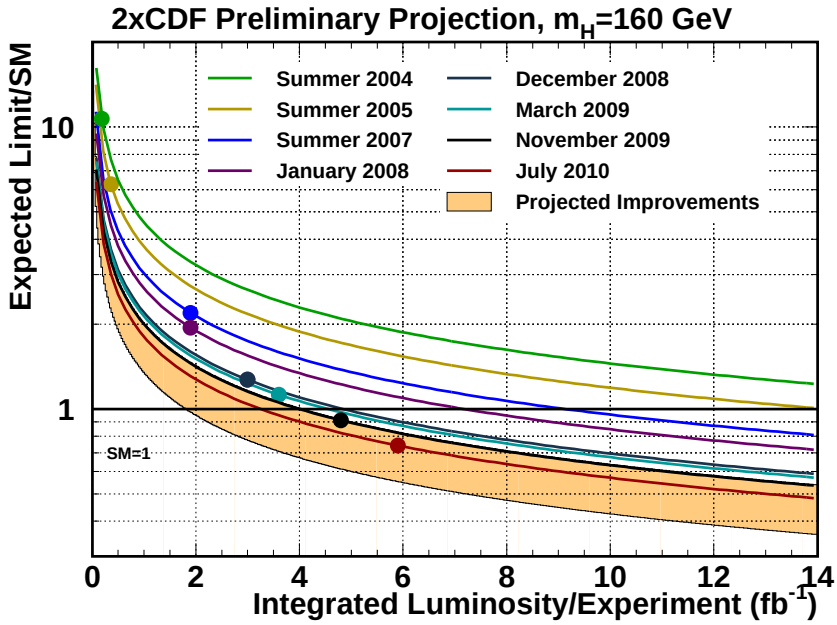

FIG. 7: Sensitivity projections and achieved sensitivities for the combined CDF Higgs boson searches, at $m_H = 115$ and 160 GeV/c^2, with a multiplier of $1/\sqrt{2}$ applied to the expected limits, to approximate the contribution of D0, assuming identical performance. The curves are proportional to $1/\sqrt{\int Ldt}$ extrapolations of the median expected limits, and each analysis update corresponds to a new point with a new curve. The light orange bands indicate ranges of possible improvements in performance, relative to the Summer 2007 sensitivity. The top of the light orange bands is a factor of 1.5 below the Summer 2007 curve, and the bottom of the light orange bands are a further factor of 1.5 below the top of the light orange bands. The points represent CDF's achieved sensitivities, where the expected limits have been divided by $\sqrt{2}$.

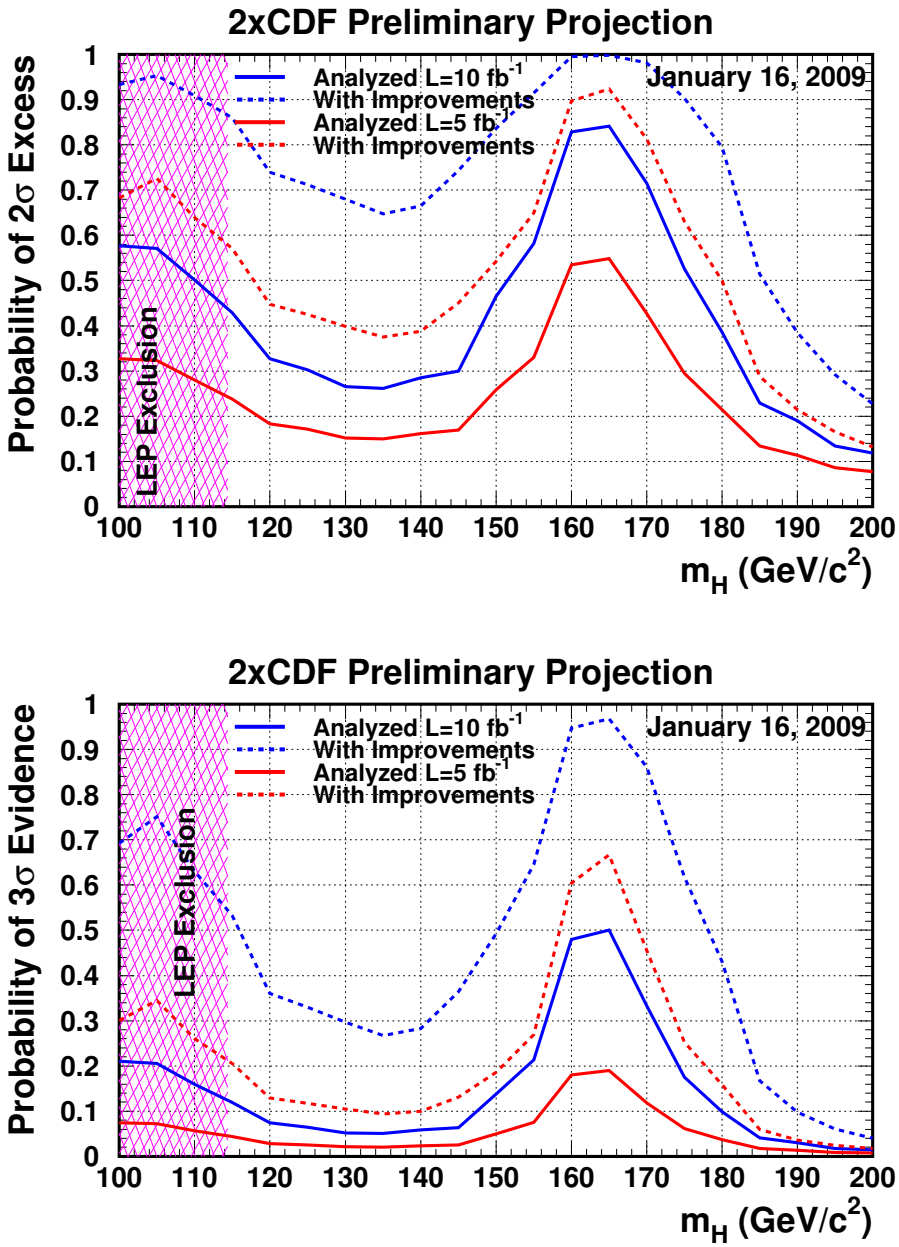

FIG. 8: Sensitivity projections as functions of m_H. These graphs show the chances of observing a 2σ excess (top) or a 3σ evidence (bottom), as functions of m_H, assuming a Higgs boson is present with production cross sections and decays at their SM values. CDF and D0 are assumed to contribute equally. The solid lines correspond to current performance as described in this note, and the dashed lines correspond to a performance level which corresponds to the bottom of the light orange bands in Figure 7. No account is taken of the data already collected and analyzed; existing excesses and deficits in the data do not affect these sensitivity projections. Two luminosity scenarios are considered: 5 fb^{-1} of analyzed luminosity per experiment (red lines) and 10 fb^{-1} of analyzed luminosity per experiment (blue lines).